X-band Digitization Systems Aspects and Filters for MeerKAT Radio Astronomy Receiver.

Jocias A. Malan

Faculty of Engineering and Build Environment

University of Cape Town

A thesis submitted for the degree of

Master of Science (Engineering)

March 2017

Dedication

I dedicate my dissertation work to my wife, Mandy and my two children Shiri and Zack. I give all the glory to my Lord and Saviour Jesus Christ.

Declaration

I know the meaning of plagiarism and declare that all the work in the document, save for that which is properly acknowledged, is my own. This thesis/dissertation has been submitted to the Turnitin module (or equivalent similarity and originality checking software) and I confirm that my supervisor has seen my report and any concerns revealed by such have been resolved with my supervisor.

Signed by candidate

Signature removed

25 May 2017

Acknowledgements

- I wish to thank Professor Riana Geschke for her mentorship and guidance.
- I wish to thank my colleagues at Square Kilometre Array project in South Africa (SKA SA) for their assistance and support.
- I acknowledge the National Research Foundation (NRF) for funding my project.

Abstract

The MeerKAT Radio Telescope is a 64 element antenna array under construction in South Africa. This array will be used to observe radiation from celestial sources at radio frequencies. Once completed, this radio telescope will be the largest and most sensitive radio telescope in the Southern hemisphere. MeerKAT is being designed to observe radio signals produced by celestial sources at UHF-, L-, S- and X-band frequencies.

With the development of the X-band receivers for MeerKAT scheduled to start in the near future, research is required to determine an optimum receiver design for this frequency band. There are two architecture options available for digitization of this band namely direct digitization of the entire band or digitization of a portion of the frequency band using a heterodyne configuration.

In this thesis, both these options are investigated to determine the feasibility of both these architectures. A key outcome of this investigation will be the derivation of the specifications of the anti-aliasing filter used in a direct digitization receiver as well as the image reject filter used in the heterodyne receiver. The design of a wideband microwave filter capable of meeting these specifications is also presented. To conclude this investigation, the impact of the designed filter on the performance of the system is presented.

Contents

List of Figures

Chapter 1

Introduction

This thesis investigates two digitization options which can be used in the receiver architecture of the MeerKAT telescope. The first option is a direct digitization receiver and the second a heterodyne receiver. These receiver architectures must be suitable for operation at the extended X-band frequency range of 8 to 14.5 GHz as required by the MeerKAT radio telescope. In this introduction a brief background to the project is given. Thereafter the objectives for this thesis are identified. An outline of the contents of the thesis is also given in this introduction.

1.1 Background

The 64 element radio astronomy antenna array known as MeerKAT, is currently being constructed in the Northern Cape Province of South Africa [3]. This array is designed to observe radio signals produced by celestial sources at UHF-, L-, S- and X-band frequencies (refer to table 2.1 for definitions of bands). The first phase of the project was to build receivers for the UHF-, L- and S-band while the X-band design has been postponed to the second phase of the project. In preparation for the start of the X-band receiver development, research is required to determine the various architecture options for the X-band receiver.

1.2 Objectives

In this thesis two possible receiver architectures are considered as possible solutions to perform digitization of the specified frequency range. The first option is to directly digitize the entire frequency range. The second option is to down convert a portion of the specified frequency band to some suitable Intermediate Frequency (IF) before digitization.

The objective of this thesis is to evaluate the feasibility of both these architecture options. Key system design parameters such as Analogue to Digital Converter (ADC) sample rates, Local Oscillator (LO) and IF frequencies are evaluated as part of this investigation. A key outcome of this investigation is the specification of both the anti-aliasing and image reject filters required by these two architecture options.

The next objective will be to design a microwave filter based on these specifications. The goal will be for this filter to be used in both applications as either an anti-aliasing or an image reject filter. The impact of the designed filter response on the two types of receivers is also investigated.

1.3 Thesis Outline

This thesis is organized in the following manner:

Chapter 2 provides a high level introductory overview of radio astronomy with particular focus being given to the MeerKAT telescope and the science which is being planned for the X-band receiver.

Chapter 3 provides an overview of the signal chain of the MeerKAT Telescope.

Chapter 4 provides a detailed analysis of a direct digitization receiver with the main focus being on determining the sample rate of the ADC as well as the requirements of the anti-aliasing filter required for direct digitization systems.

Chapter 5 provides a detailed analysis of a heterodyne receiver. In this chapter specific focus is given on the selection of LO and IF frequencies. Analysis is also done to determine the impact of the various mixing products as well as the image frequency on the performance of the system. The specifications of an image reject filter required for this architecture is also derived.

Chapter 6 combines the requirements of the anti-alias and image reject filters for the two architectures into one set of requirements for a microwave filter which can be used for both architectures. Investigation is done into finding a suitable filter topology which can meet these specifications. Finally a filter is designed and constructed based on the selected topology.

Chapter 7 provides a high level system design of the receiver based on the two architectures. Some of the major components required by the system are also identified. The impact of performance of these components as well as the designed filter on the system is also presented.

Chapter 8 presents the conclusions and recommendations of this thesis.

Chapter 2

Introduction to Radio Astronomy

Since the first detection of radio signals generated by cosmic sources, the science of radio astronomy has expanded tremendously over the last century. This expansion has led to the construction of many radio telescopes across the world. Many observatories across the globe have been constructed to observe the radiation from the universe, using these very sensitive radio telescopes. As an introduction to this thesis, a broad overview of radio astronomy is given including an introduction to the largest and most ambitious radio astronomy project ever constructed namely the Square Kilometre Array (SKA). A brief overview is given of cosmic signals and their properties which is important to understand when designing receiver systems for radio telescopes.

2.1 Background of Radio Astronomy

Radio astronomy is a sub field of astronomy that studies celestial objects at radio frequencies [4]. The first detection of a celestial object was made by Karl Jansky in 1931, who detected radiation generated by the Milky Way. Since then, detections of many radio sources have been done. These include stars, galaxies, quasars, pulsars and masers. One of the key properties of celestial sources is

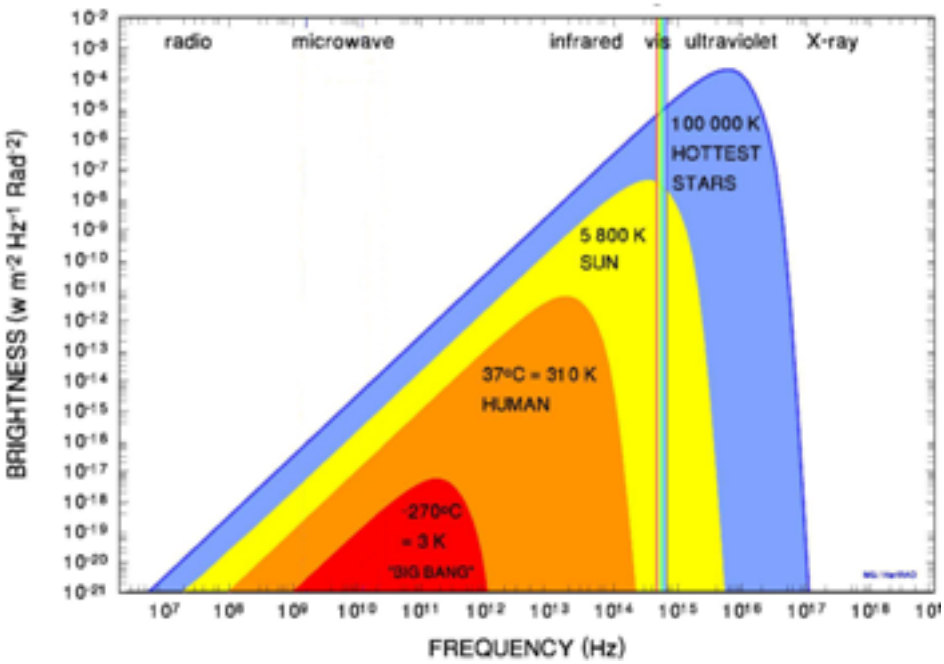

Figure 2.1: Source brightness as a function of frequency.
Image from presentation by Dr.M Gaylard, HartRAO

that the source radiates electromagnetic energy over a wide frequency range as shown in figure 2.1. In this figure, the radiation intensity of the hottest stars, the sun, a human body and left over cosmic radiation from the Big Bang is shown as a function of frequency and wavelength [5]. Visible light emitted from a source, such as a star or the sun, contains only some of the information regarding the properties of that source. Much more can be determined of the source by observing over the full spectrum generated by the source. Refer to section 2.5 for more detail on the properties of cosmic signals.

Observatories have been constructed throughout the world that are dedicated to observing sources at specific portions of the spectrum. One such an example is the High Energy Stereoscopic System (H.E.S.S) located in Namibia [6] which observes sources at gamma-ray frequencies. For radio astronomy, observations are however typically done at frequencies from 100MHz to about 100GHz.

Observations for radio astronomy are performed by collecting cosmic radiation using large parabolic antennas. These signals are then converted to electrical

Figure 2.2: Arecibo observatory in Puerto Rico.
Image by Arecibo Observatory

signals using very sensitive radio front-ends and receivers. Electrical signals are then amplified and filtered to select the frequency band of interest before being digitized for further processing. In order to achieve the sensitivity requirements needed to detect cosmic signals, the antennas used by observatories are typically designed to be as large as possible. The output power delivered by an antenna is given by the following equation

$$P_o = P_{rad} \times A_{eff} \tag{2.1}$$

From this equation it can be seen that, the output power delivered by an antenna to a load, P_o in Watts, is a function of the power density of the radiated signal, P_{rad} in Watts per square meter, that arrives at the antenna and the effective area, A_{eff} in square meter, of that antenna. The larger the effective area of the antenna, the more power will be delivered to the load. One of the most famous examples of such an observatory is the Arecibo Observatory in Puerto Rico where a 305 metre diameter radio antenna was constructed inside a massive sinkhole [7]. A photo of this observatory is shown in figure 2.2.

To construct these very large antenna structures is very difficult and expensive since these structures require specialized infrastructure and mechanical structures to support the weight of these antennas. Similar system sensitivity can be achieved by adding signals form an array of antennas in phase. This type of radio astronomy is referred to as an interferometer [4] and refers to an array of

Figure 2.3: Y-shaped configuration of the VLA.
Image by NRAO/AUI

antennas used to observe the same source by adding signals from all the antennas in the array in phase such that the combined signal approximates that of a signal produced by a large antenna. Instead of one large antenna many smaller and cheaper antennas can be constructed and placed at some distance from each other. The signals produced from all these smaller antennas can be coherently added after corrections have been made for differences in phase due to the physical separation of these antennas. The difference in phase between antennas is also used to resolve the exact position of the source on the sky [4]. An example of such an interferometer is the Karl G. Jansky Very Large Array (VLA) located in New Mexico, USA [8]. Interferometry is discussed further in section 2.3.

This array comprises of 27 25-metre radio telescopes which are arranged in a Y-shape configuration as shown in figure 2.3. In this configuration, the maximum distance between antennas is 36km. This allows scientists to determine the position of sources in the sky to the same accuracy as would be possible with a theoretical antenna that has an diameter of 36km. Similarly the sensitivity of this system is equivalent to that which can be achieved by an single dish parabolic antenna with with diameter of 130m [8].

2.2 Introduction to SKA

The Square Kilometre Array (SKA) is an international project which aims to construct the world's largest radio telescope with an aim to achieve an overall antenna collecting area of one square kilometre [9].The SKA aims to achieve this goal by building an antenna array of approximately 2000 antennas which will be located in Southern Africa and Australia. As a technology pathfinder to this project the National Research Foundation (NRF) of South Africa, has constructed a technology demonstrator instrument in the Karoo area of South Africa. This technology demonstrator will be incorporated into phase one of the SKA project. This instrument is called MeerKAT and refers to a 64 element antenna array located near Carnarvon in the Northern Cape province of South Africa [3].

The antenna used by MeerKAT is an offset Gregorian topology. An offset Gregorian antenna is a parabolic antenna that consists of a main parabolic reflector which focuses electromagnetic waves onto a secondary concave shaped reflector which in turn focus the electromagnetic waves on the system front-end [10]. This design ensures an unobstructed beam for observations of celestial objects [11]. The MeerKAT antenna uses a main reflector with a diameter of 13.5m and sub-reflector diameter of 3.8m.

The antenna will be fitted with four different receivers which will allow for the observation of celestial sources at UHF-, L-, S- and X-band frequencies. An antenna fitted with front-ends and receivers is called a Receptor. A picture of one of these Receptors is shown in figure 2.4.

As of December 2016, 21 of these Receptors have been constructed. These antennas have been fitted with the L-band front-ends and receivers. The development of the UHF- and S-band front-ends and receivers are also in progress while the development of the X-band front-end and receiver is planned for the near future. The work of this thesis will serve as an input to the X-band development.

The frequency bands for MeerKAT are summarized in table 2.1.

Figure 2.4: MeerKAT antenna.

Table 2.1: MeerKAT frequency bands.

Band name	Frequency range
UHF-band Frequency	580 - 1015MHz
L-band Frequency	900 - 1670MHz
S-band Frequency	1750 - 3500MHz
X-band Frequency	8000 - 14500MHz

2.3 Interferometry

As already discussed a, greater antenna collecting area can be achieved by building lots of small antennas and coherently adding the signals from these antennas. This type of radio astronomy instrument is called an interferometer. A block diagram of a two antenna interferometer is shown in figure 2.5 [4]. The two antennas are physically separated by D meters which is also known as the baseline. Cosmic electromagnetic waves reach the antennas as a planar wave since the electromagnetic wave is observed in the far filed. In this case the wave reaches antenna B before A due to the observation angle, θ, resulting in a time delay between the received signals, referred to as the geometric delay τ_g. As the earth rotates, θ changes which also results in a change in τ_g. Geometric delay, τ_g, can

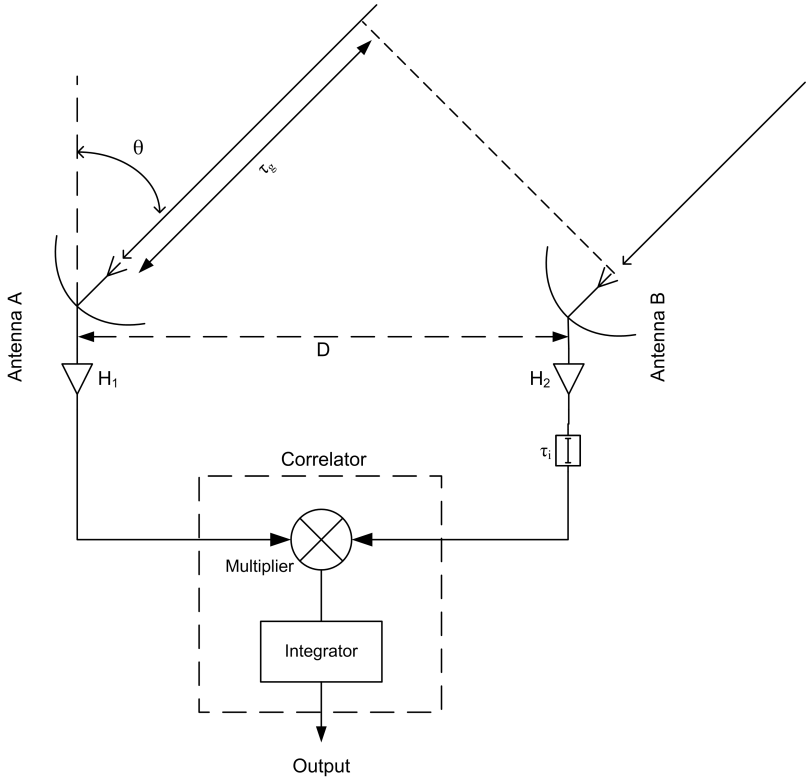

Figure 2.5: Block diagram of interferometer.
Image adapted from [4]

be calculated using the equation

$$\tau_g = \frac{D}{c} sin\theta \tag{2.2}$$

The output of these antennas is multiplied and time averaged in the Correlator. The output of the multiplier of the Correlator, F, can be calculated using equation 2.3 if the source is assumed to be radiating a sine wave at a single

frequency of f.

$$\begin{aligned} F &= 2sin\left[2\pi ft\right] sin\left[2\pi f\left(t-\tau_g\right)\right] \\ &= cos2\pi f\tau_g - cos(4\pi ft)cos(2\pi f\tau_g) - sin(4\pi ft)sin(2\pi f\tau_g) \end{aligned} \tag{2.3}$$

The second and third terms of equation 2.3 is fast varying as $f\,\tau_g << f\,t$ and can easily be filtered out leaving the fringe function given in the following equation

$$F = cos\left(\frac{2\pi D}{\lambda} sin\theta\right) \tag{2.4}$$

where λ is the wavelength in metres of the frequency at which the observation is performed.The two antennas have different components of velocity in the direction of the sources due to the rotation of the earth. The signals reaching the antennas therefore suffer different Doppler shifts [1]. When the signals are combined in the multiplying action of the receiving system, a sinusoidal output arises from the beats between the Doppler shifted signals. The variation of in τ_g is as a result of the rotation of the earth is a delay which needs to be compensated for. The method used is referred to as fringe stopping. Fringe stopping is outside the scope of this work and will therefore not be discussed further. However, the ability of the instrument to perform fringe stopping is greatly affected if there are uncontrolled variation in instrumentation delays between antennas. Variation in instrumentation delays, τ_i, can be due to temperature change or variation in manufacturing of components. This is an important aspect to be considered in the design of receivers.

[1] Change in frequency by an observer due to a source moving either towards or away from the observer.

2.4 Key Science Planned for X-band

The key science case for the X-band receiver of MeerKAT is to perform a high frequency galactic plane survey of the southern sky known as MeerGAL (MeerKAT High Frequency Galactic Plane Survey). This science case aims to perform a survey of the galactic plane over the frequency range of 10-14 GHz. The measurements which will be performed will include broadband continuum observations [1], high resolution spectral line observations [2] as well as the observation of masers [3] and Radio Recombination Lines (RRL). This survey aims to perform the deepest and most high resolution survey of the southern galactic plane at 14 GHz. MeerGAL also plans to perform observations of 12.2GHz CH_3OH masers [12]. Although the frequency range of the X-band system is from 10 -14GHz, the instantaneous or processing bandwidth required is $\geq 2GHz$.

2.5 Overview of Cosmic Signals

Voltages induced by cosmic sources do not contain information in the usual engineering sense. These signals typically have a Gaussian random noise response which is assumed to be identical to the noise generated by electronics components such as resistors and amplifiers. The characteristics of these signals are, for most sources, invariant with time. The power generated by celestial sources are measured in Jansky with 1 Jansky being equal to $10^{-26}Wm^{-2}Hz^{-1}$ or $-220dBmHz^{-1}$ [4]. Most power from sources is in the form of continuum radiation. Continuum radiation means that the power of a source shows a slow variation with frequency and may be regarded as constant over the receiving bandwidth of the instrument [4]. The Power Spectral Density (PSD) of some continuum sources are shown in figure 2.6 [1].

[1] Refers to the observation of sources with power spectrum that shows slow variation with frequency over the observation bandwidth

[2] Refers to observations of sources that shows concentrated power in a small portion of the observed bandwidth

[3] Naturally occurring source of spectral line emissions which can be generated from Comets and other cosmic sources

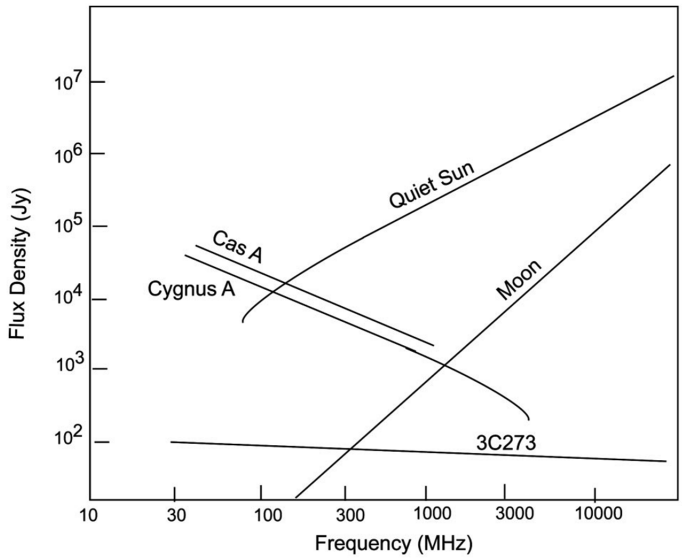

Figure 2.6: Power Spectral Density (PSD) of a continuum source [1].

Spectral line radiation is generated at specific frequencies by atomic and molecular process. A fundamentally important line is that of neutral atomic hydrogen (H1) at 1420.405 MHz. Another example of spectral line emissions is that of Helium and Methanol which radiates at 8.665 and 12.179GHz respectively. The frequency of these spectral lines is within the frequency range of the X-band receiver. A list of some of the most important molecular lines are listed in the table 2.2 [4].

Table 2.2: Some important radio lines.

Chemical name	Chemical Formula	Frequency (GHz)
Deuterium	D	0.327
Hydrogen	H1	1.420
Methyladyne	CH	3.335
Helium	He	8.665
Methanol	CH_3OH	12.179
Water	H_2O	22.235

The frequency bandwidth of these lines is negligibly small, but the line is spread in frequency as a result of red shift. Redshift refers to the increase in wavelength, or decrease in frequency, of electromagnetic waves due to the source

moving away from the observer. The redshift factor, z, of a source is a comparison between the frequency at which the source radiates compared to the frequency at which the source is observed. This relationship is given by equation 2.5.

$$z = \frac{f_{rad} - f_{obs}}{f_{obs}} \tag{2.5}$$

where f_{rad} is the radiation frequency of the source and f_{obs} is the observation frequency. It can be seen from this equation for $z = 1$, the observation frequency is 0.5 f_{rad}. Radio astronomers can observe sources at redshifts as high as $z = 5$ [13] which explains the need for wide bandwidth and continuous frequency coverage of the spectrum using various receivers. As an example the natural resonance frequency of a water molecule is given by table 2.2 as 22.235 GHz which is way outside the frequency range of the X-band receiver. If this frequency is red shifted by $z = 1$ the observed frequency will be 11.118 GHz which is now inside the received band.

Another important characteristic of cosmic signals is that these signals are propagated such that the observed polarization, geometric orientation of oscillation, of the signal is mainly linear. Electric and magnetic fields generated by an electromagnetic wave are positioned orthogonally to each other along the direction of propagation in linearly polarized signals. A signal is said to be vertically polarized if the electric field oscillates in an up/down motion as observed by the receiving antenna. Conversely the signal is said to be horizontally polarized if the signal oscillates in a left/right motion as observed by the receiving antenna. This concept is illustrated in figure 2.7. Since very little information regarding the cosmic source of an observed signal is known, radio telescopes observe received cosmic signals in both horizontal and vertical polarizations. This enables scientists to determine the polarization state of the source.

The system therefore needs to be able to receive and process cosmic signals which can either have a continuum power spectrum or can be in the form of definite spectral lines as shown in table 2.2. In addition to this the system also needs to observe in both horizontal and vertical polarizations. Chapter 3 describes how the properties of these signals are used to determine the design specifications

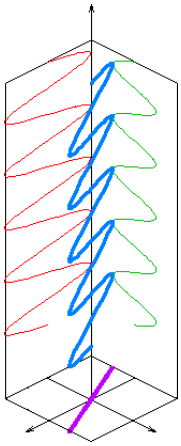

Figure 2.7: Linear polorization of electromagnetic wave [2].

of the MeerKAT X-band receiver architecture.

2.6 Summary

In this chapter an overview of radio astronomy is given. This overview has led to the identification of some very important characteristics of cosmic sources and radio astronomy instruments which needs to be considered when designing receivers for radio astronomy applications. These are summarized below. These characteristics will be expanded on in chapter 3.

- Signals produced by celestial sources are similar to the noise produced by electronics
- Radio astronomy sources can be either broadband continuum sources or they can radiate at definite spectral lines
- The observation frequency of radio sources can differ from the radiation frequency due to redshift. This necessitates the design of very wideband receivers.
- Variation in instrumental delays due to temperature changes as well as

manufacturing tolerances affects the ability to perform fringe stopping in interferometers.

- The instantaneous or processing bandwidth is less than the full observation bandwidth

Chapter 3

Receiver Signal Chain Analysis

The analogue signal chain of a radio telescope has a major impact on the overall performance of the system. It ultimately determines the sensitivity of the telescope. In this chapter, a detailed analysis is given of the analogue signal path to determine the key requirements which drives the design of the receiver.

3.1 Signal Chain of MeerKAT Telescope

A block diagram of the typical analogue signal chain is shown in figure 3.1 for a direct digitization receiver and in figure 3.2 for a heterodyne receiver. The analogue part of the signal path is divided into two subsystems namely the front-end sub-system and the receiver subsystem. The front-end and the receiver is connected via one metre of coaxial RF cable. These two sub-systems are discussed in the subsequent sections.

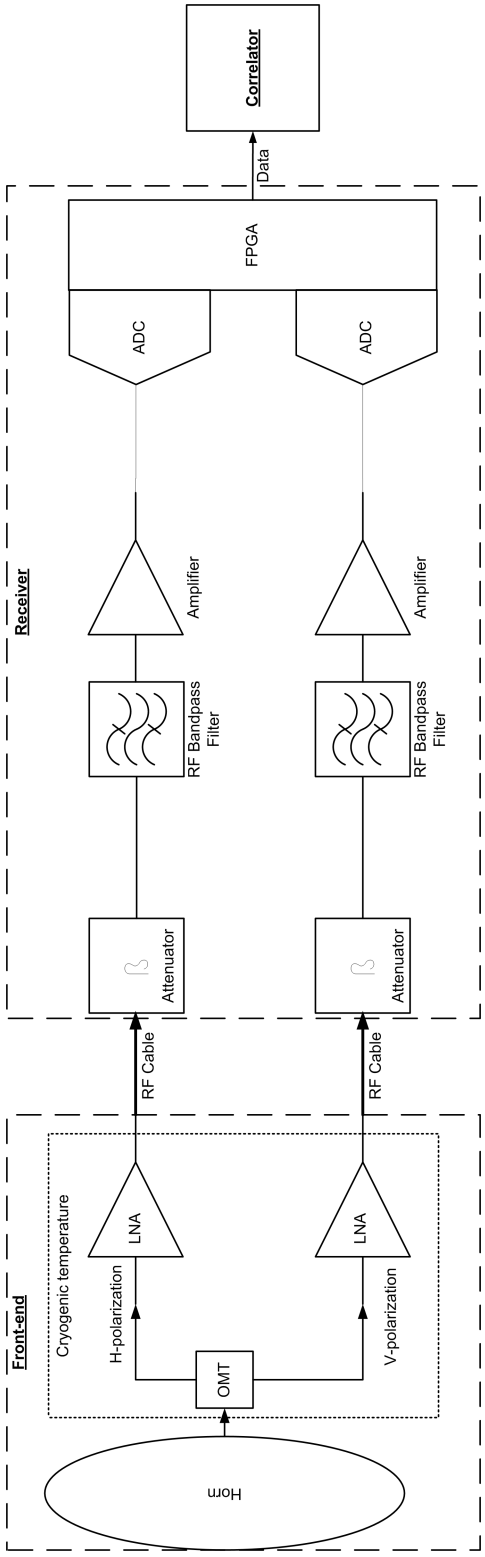

Figure 3.1: Block diagram of MeerKAT signal chain for direct digitizing receiver.

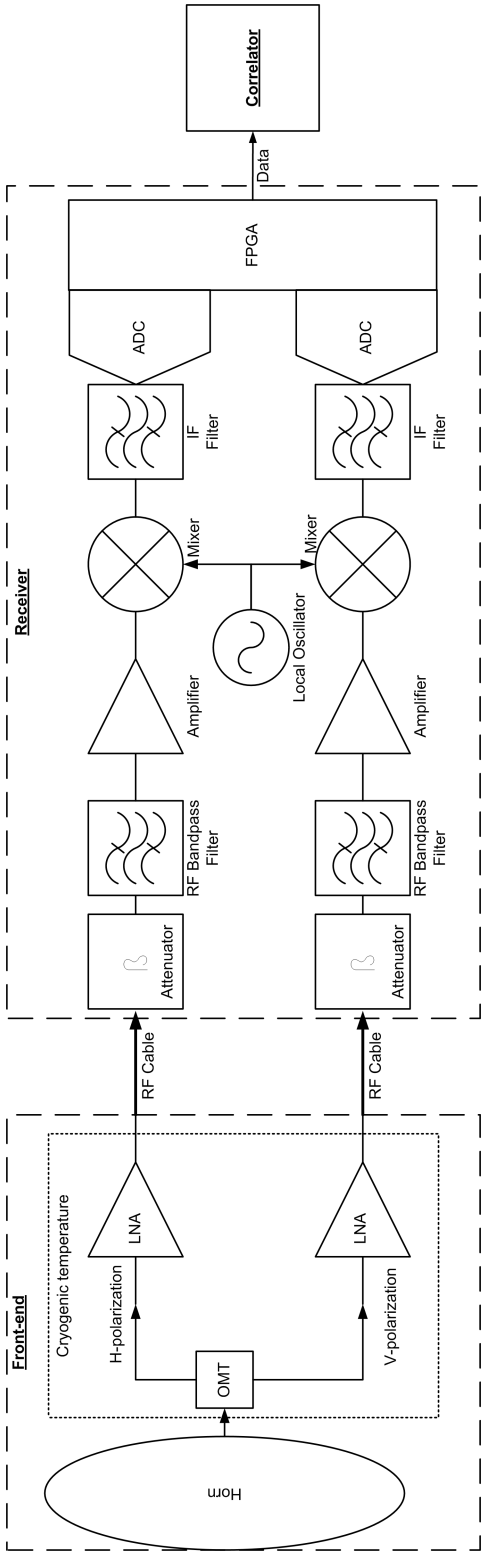

Figure 3.2: Block diagram of MeerKAT signal chain for heterodyne receiver.

3.1.1 Front-end

As already discussed in section 2.2, cosmic signals are focused on to the horn assembly of the front-end using the combination of the main- and sub-reflector of the offset Gregorian MeerKAT antenna shown in figure 2.4. The front-end collects the celestial electro-magnetic (EM) waves and converts these to electrical format using an Ortho-Mode Transducer (OMT). This OMT is a waveguide component used to separate the linearly polarized electro-magnetic waves emitted by celestial sources into two channels which contains the horizontal and vertical polarized signals.

The horn of the front-end plays a vital role in shaping and tapering the antenna beam. Incorrect horn shape can cause loss in power and increase in antenna side lobes. These problems can be avoided by matching the shape of the horn to that of the sub reflector [11].

Once the EM signal is converted to an electrical microwave frequency [1] signal, this signal is amplified by a Low Noise Amplifier (LNA) as well as a second amplification stage before entering the receiver subsystem. The front-end plays a vital role in the overall sensitivity of the radio telescope as noise generated by this sub-system will significantly degrade the overall noise figure of the system. For this reason radio astronomy telescopes typically deploy front-ends which operate at below cryogenic temperatures. This means that critical components inside the front-end, namely the OMT and LNA, is cooled to $< 93.15K$ [2]. The typical temperature for the MeerKAT front-end is 70K.

The reason for the cooling of these critical components to such extremely cold temperatures is to reduce the equivalent system noise temperature T_{sys} of the instrument. Unwanted noise power, P_n measured watts, introduced by electronic components such as OMT and LNAs can be calculated using the following expression:

[1] Signal with frequency of 300MHz to 300GHz

[2] Definition of cryogenic temperature according to United States National Institute of Standards and Technology

$$P_n = k\,T_{sys}\,B \tag{3.1}$$

Where $k = 1.38 \times 10^{-23}$ (Joules / Kelvin) known as Boltzmann constant, T_{sys} equivalent noise temperature (Kelvin) and B is the total bandwidth, in Hertz (H), over which the noise power is measured. It is clear from this equation that unwanted noise power generated by the system can be reduced by decreasing the noise temperature of the system which explains why radio astronomy receivers typically operate at cryogenic temperatures.The typical noise temperature of the entire front-end is $\leq$ 30 kelvin (K). Based on this analysis, any cosmic signal presented at the input to the front-end needs to be larger than the noise power generated by the front-end in order for the system to be able to detect it. For this front-end the noise power in 1 Hz bandwidth can be calculated using 3.1 as 4.14×10^{-22} Watts or $-183.83dBm$. The key specifications of the front-end sub-system is given in table 3.1 [14].

Table 3.1: Front-end key specifications.

Parameter	Specification
Frequency range	8-14.5GHz
Gain	46dB
Noise temperature	$\leq 30K$

3.1.2 Receiver

The main purpose of the receiver subsystem is to digitize the signal produced by the front-end. This can be done either by designing a receiver which digitizes the band of interest directly, without any down-conversion in frequency, or by designing a receiver that uses a heterodyne architecture to frequency translate the band of interest to a suitably lower frequency IF before digitization. In both these cases the signal produced by the front-end needs to be conditioned to be compatible with specifications of the Analogue-to-Digital Converter (ADC) which is being used. Conditioning of the signal prior to conversion can include

the following:

1. Bandpass filtering of the signal to select only the band of interest while rejecting unwanted signals
2. Bandpass filtering of the signal to prevent aliasing of unwanted signals during the conversion process.
3. Down-conversion of the band of interest to a suitable IF frequency.
4. Gain adjustment of the signal to ensure that the power level of the signal entering the ADC is correct.

Once signal conditioning has been done, the ADC converts this band limited signal into digital format at a rate which depends either on the bandwidth of the IF signal if down-conversion is done or by the Nyquist zone which is sampled in the case of direct digitization. The digitized data is then arranged in Ethernet packets by the Field Programmable Gate Array (FPGA) and transmitted to the correlator via optical Ethernet interfaces. The correlator receives data from all the receptors and determines the signal path delays between them. The correlator then compensates for these delays before adding the signals from all receptors in phase as if the signals were produced from one large antenna.

Both the front-end and the receiver are physically located on a platform which is located between the main reflector and the sub-reflector of the Receptor shown in figure 2.4. There is no environmental protection for these sub-systems resulting in very strict environmental requirements in which these systems must operate. The physical realization of the receiver for the current L-band is shown in figure 3.3.

3.2 Functional View of Receiver Signal Path

In this section a functional view of the signal path inside the receiver is presented. By analyzing the functions that the receiver needs to perform, key specifications

Figure 3.3: Physical view of the equivalent L-band receiver.

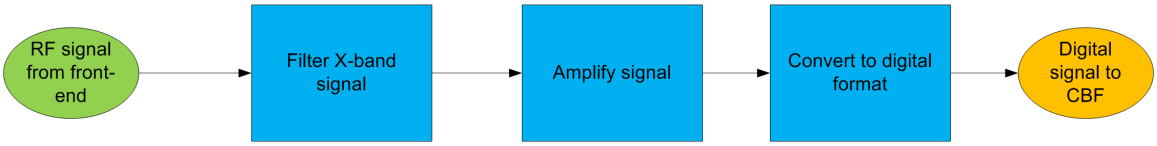

Figure 3.4: X-band receiver functions.

can be identified which will ensure that the overall performance expectation of the system is met [15]. The functional flow diagram of the X-band receiver is shown in figure 3.4. Each of these functions are described in the subsequent sections.

3.2.1 Filter X-band Signal

3.2.1.1 Frequency Response

Filtering requirements for the receiver is heavily dependent on the architecture chosen for the digitization. The filter requirements for a heterodyne architecture is very different form the filter requirements of the direct digitization architecture. For a heterodyne receiver, an image reject filter is required, while an anti-aliasing

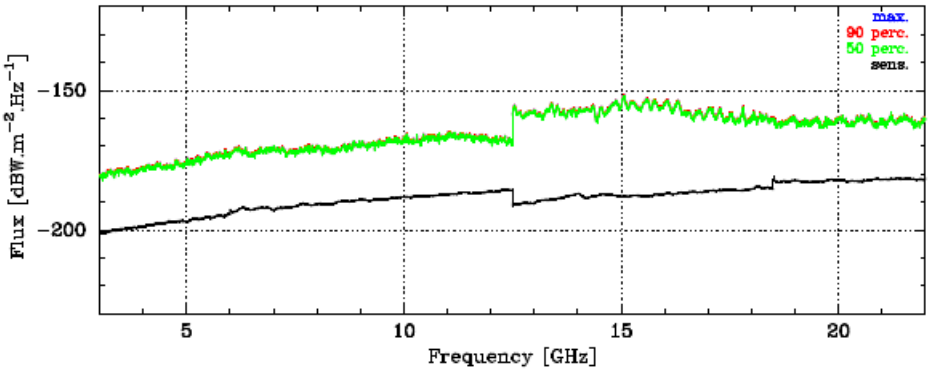

Figure 3.5: Terrestrial X-band interference measurement on MeerKAT site. *Black trace represents the noise floor of the measurement system. Measurement data shown by green and red traces.*

filter is required for a direct digitisation architecture. The specifications of these filters are derived in chapters 4 and 5 respectively. The main aim of this section is to determine filter requirements based on system effects like interfering signals.

The frequency range for the X-band front-end of MeerKAT is 8-14.5GHz as given in table 2.1. This frequency range therefore defines the passband of the filter. To understand the specifications on the stopband of the filter, an audit needs to be done on unwanted signals present in the environment which can enter the signal path. If the power levels of these signals are large enough, it can cause the receiver to operate in a non-linear state which will reduce the overall system performance. Unwanted signals can either be generated by terrestrial sources such as point to point communication systems, or can be generated by space borne sources such as satellite communication systems.

Measurements on the MeerKAT site [16] was performed to determine the levels of unwanted terrestrial signals in the specified frequency range. The result of this measurement is shown in figure 3.5. It is clear from these measurements that there is no need to provide out of band rejection for unwanted terrestrial signals over the frequency range of 5 to 22GHz.

Currently no measurements have been performed on the site to determine the levels of space borne unwanted signals. Frequency allocations by the International

Table 3.2: Satellite frequency utilization.

Application	Frequency range
Broadcast Satellite Service(BSS) uplink	5.9-6.4GHz
Space research	8-9 GHz
Fixed Satellite Services (FSS)	10.7-11.7GHz
BSS downlink	11.7 - 12.2 GHz
Ku-band uplink	14.5-14.8 GHz
Alternate Ku-band BSS uplink	17.3-18.1 GHz

Telecommunication Union (ITU) do however specify the frequency bands that are being utilized by satellites. Table 3.2 list the most prominent frequencies close to the passband [17] as provided by ITU. Most of the frequencies are inside the band of interest and can only be avoided by ensuring that the antennas do not point directly to these satellites during observations. The out of band signals needs to be rejected by the filter of the receiver.

In order to determine the exact amount of suppression required for the out of band signals actual measurements must be performed to determine the level of these signals on site. Since this measurement is outside the scope of this work, signals at 7 and 15 GHz are specified to be suppressed by $\geq 15dB$ [14].

An estimate of the filter order required to achieve the stopband suppression can be made for a Chebyshev low pass filter prototype using the following equation [18]:

$$n \geq \frac{cosh^{-1}\sqrt{\frac{10^{0.1\,L_{AS}-1})}{10^{0.1\,L_{AR}-1}}}}{cosh^{-1}\,\Omega_s} \tag{3.2}$$

where L_{AS} is the required stopband rejection and L_{AR} is the required passband ripple in dB. Ω_s is the ratio between the upper passband frequency f_U and the stopband frequency f_S given by the following equation:

$$\Omega_s = \frac{f_S}{f_U} \tag{3.3}$$

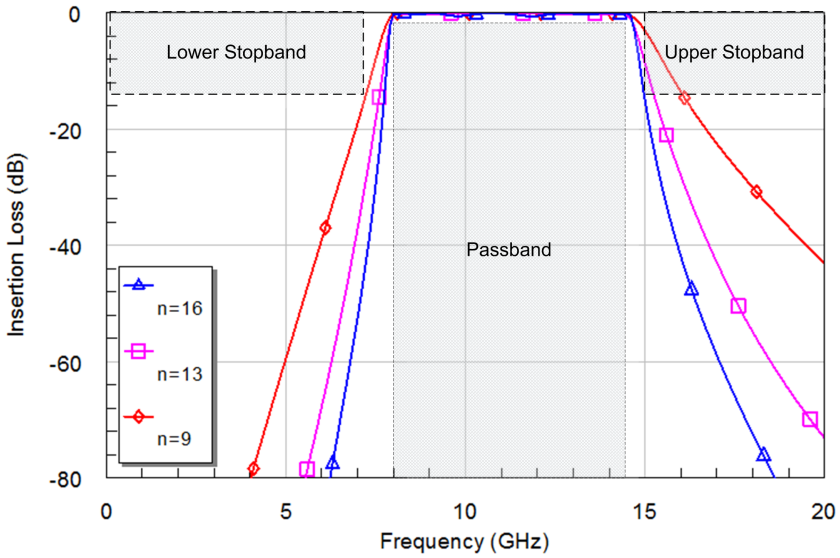

Figure 3.6: RF Filter response.

For this application, an 16th order Chebyshev filter will be required given that $L_{AS} = 15$ dB at 15GHz and assuming a passband ripple of $L_{AR} = 0.1$ dB. The frequency response of such a filter is shown in figure 3.6. The filter response of a 9th and 13th order filter is also shown on the same graph. It is clear from this graph that the lower stopband rejection specification can be met by a 13th order filter, but this filter will not achieve the upper stopband frequency specification.

3.2.1.2 Passband Ripple

Within the passband of the receiver, the amplitude flatness needs to be controlled such that the the ripple is less than 2dB peak to peak [14]. Ripple within the passband can be caused by standing waves due to impedance mismatch, filter design constraints and due to the frequency response of components such as amplifiers and mixers.

A good input match is required to ensure that no standing waves [1] are gener-

[1]Superposition of an incident and reflected wave on a transmission line. Reflected wave is caused by an impedance mismatch.

ated on the interface between the front-end and the receiver. A good input match is ensured by placing an attenuator at the input of the receiver [19]. Standing waves on transmission lines are normally caused by mismatches between a source and a load. These standing waves can result in undesired ripple inside the passband of the system and therefore need to be carefully managed. The amplitude ripple which can be induced due to impedance mismatch between the front-end and the receiver can be calculated using equation 3.4 [19].

$$A_{pk-pk} = 20\,log_{10}\left[1 + |\Gamma_{FE} \times \Gamma_{Rx}|\right] - 20\,log_{10}\left[1 - |\Gamma_{FE} \times \Gamma_{Rx}|\right] \tag{3.4}$$

If the front-end and the receiver is assumed to have a reflection coefficient of $\Gamma = 0.177$, the peak to peak amplitude variation due to impedance mismatch will then be approximately $0.6dB_{pk-pk}$ across the passband. Reflection coefficients can be converted to return loss which is a more commonly used parameter using equation 3.5. $\Gamma = 0.177$ therefore equates to 15dB return loss.

$$RL_{dB} = 10\,log_{10}(\Gamma^2) \tag{3.5}$$

Components such as the amplifiers and mixers will typically not produce passband ripple, but rather a linear slope over frequency. Since ripple due to impedance mismatch already contributes 0.6 dB, other contributing factors to passband ripple need to be constrained such that they do not degrade the passband response by more than $3.4\,dB_{pk-pk}$. This specification has a significant impact on the choice of filter topology as well as selection of amplifiers and other microwave components as will be shown in chapter 7.

3.2.1.3 Instantaneous Bandwidth

From the science cases discussed in section 2.4 the instantaneous bandwidth needs to be $\geq 2GHz$. The instantaneous bandwidth requirements can easily be achieved in the case where direct digitization is performed. In the case where down-conversion is performed, a trade-off needs to be done between image rejection and instantaneous bandwidth. This tradeoff is discussed in detail in chapter 5.

3.2.2 Amplify Signal

3.2.2.1 Receiver Gain

In order to determine the gain of the receiver, the output power level from the front-end system must first be determined. The minimum output power from the front-end, P_{FE} in dBm, is a function of the system noise temperature, gain and the bandwidth and can be calculated using the following equation:

$$P_{FE} = 10 * log_{10}\left[\frac{kTB}{1 \times 10^{-3}\,W}\right] + G_{FE} \tag{3.6}$$

where K is Boltzmann constant (1.38×10^{-23}) , T is the system noise temperature, B is the processing bandwidth and G_{FE} is the gain of the front-end in dB. For the specifications of the front-end given in 3.1, the output power level of the front-end is $-44.8\,dBm$. This signal needs to be amplified by the receiver such that the input power level to the ADC's 12 dB below Full Scale (dBFS). By ensuring the AC input is operating at this power level, the sampling efficiency of the system will meet specification [14]. This power level determines how many of the ADC bits are toggling when the minimum power level is present at the input to the ADC. Assuming that the full scale power level of the ADC is 0dBm, the gain of the receiver can then be calculated using the following equation:

$$G(dB) = P_{ADC} - P_{nom} = 32.8dB \tag{3.7}$$

3.2.2.2 Noise Temperature

As previously stated, the noise temperature performance of radio telescopes have a direct impact on the sensitivity of the overall system. For this reason a key design factor of the front-end is to minimize the noise figure. The choice of Low Noise Amplifier (LNA), physical operating temperature as well as losses in front of the LNA all contribute to the degradation of the noise figure. The contribution of the receiver to the overall system temperature is however minimal since the receiver is preceded by the front-end which has a significant amount of gain (46dB).

In the case of the receiver, the first component in the line-up will not be a low noise amplifier, but rather a wide band attenuator as already discussed in section 3.2.1.2. This attenuator is followed by a filter with insertion loss. To understand the impact of the losses inside the receiver on the overall noise figure performance of the system, a noise figure analysis of a cascaded system shown in 3.2 needs to be performed. The noise figure of the cascaded front-end and receiver can be calculated using the following equation [19]:

$$F = F_{FE} + \frac{F_{Rx}}{G_{FE}} \tag{3.8}$$

where F_{FE} and F_{Rx} is the noise factor of the front-end and receiver respectively, while G_{FE} is the gain of the front-end. The conversion between noise temperature and noise factor is given by the following equation:

$$F = 1 + \frac{T_{FE}}{T_0} \tag{3.9}$$

where T_{FE} is the equivalent noise temperature of the front-end and T_0 is the reference temperature which is 290K. Given the specification listed in table 3.1 as well as equation 3.9 the noise factor of the front-end is calculated as 1.1034 or 0.428dB.

In the case of the receiver, the insertion loss of the attenuator and the filter adds to the noise figure of the amplifier [19] shown in figure 3.2.For noise analysis purposes, the attenuator, filter and amplifier can be therefore be equated to a single amplifier with gain of G_{Rx} and noise figure of $NF_{Rx} = A + IL + NF_{amp} = 8 + 2 + 3 = 13\,dB$. Using equation 3.8, the cascaded noise factor can now be calculated once NF_{Rx} has been converted to linear form. The resultant cascaded noise factor of the front-end and the receiver is calculated as 1.1037 or 0.429dB. From this analysis it is clear that an attenuator at the input to the receiver followed by a filter only degrades the overall noise figure of the system by 0.027% by less than 0.001dB.

3.3 Key Design Requirements

The analysis performed in this chapter has led to the identification of key specifications of the receiver which is listed in table 3.3. This table also lists some other key specifications which was not explicitly derived as part of this analysis, but are important specifications which needs to be considered as part of the design of the receiver [14]. These include:

- Signal to Noise Ratio (SNR) Ratio of the signal power to noise power in the receiver.
- Spurious Free Dynamic Range (SFDR) Signal strength ratio between the

Table 3.3: Key performance requirements.

Parameter	Specification
Frequency range	8-14.5GHz
Stop band rejection	15 dB
Lower stopband frequency f_l	7GHz
Upper stopband frequency f_u	15GHz
Passband ripple	$\leq 3.4\,dB_{pk-pk}$
Instantaneous bandwidth	$\geq 2\,GHz$
Gain	20.7 (dB)
SNR	$\geq 23dB$
SFDR	$\geq 55\,dBc$
Group delay	$\leq 3.5ns$
Returnloss	$\leq -15dB$

fundamental signal to the strongest spurious signal.

- Group delay Time delay as a function of frequency of signals passing through a device such as an amplifier or filter.

These specifications will be extensively used in the next chapters where the two digitization architecture options of the receiver will be discussed and analyzed.

Chapter 4

Direct Digitization

There are two possibilities that need to be evaluated for the sampling of the specified frequency range, namely direct digitization of the spectrum or down-convertion of a portion of the spectrum by means of a heterodyne receiver. In this chapter direct digitization of the band is discussed. As an introduction to this chapter an overview of sampling theory is also presented.

4.1 Sampling Theory

4.1.1 Baseband Sampling

Sampling of a continuous time signal, $x(t)$, at a periodic sample rate of $T = 1/f_s$ results in a discrete time sequence, x_T, being derived for n number of samples. At any value of n, the discrete time sequence relates to the continuous time signal as $x_T(n) = x(nT)$ [20]. During the sampling process, each sample is attached to (multiplied with) a direct delta function, $\delta(\frac{t}{T} - n)$, which leads to the expression

for the sampled signal being given by equation 4.2 [20].

$$x_T(t) = \sum_{n=-\infty}^{\infty} x(nT)\delta(t/T - n) \tag{4.1}$$

In order to get a spectral view of the sampled signal, a Fourier transform of $x_T(t)$ can be taken. This Fourier transform is given by equation 4.2 [20].

$$\mathcal{F}X_T(\omega) \quad = \sum_{k=-\infty}^{\infty} \mathcal{F}X(\omega - k\Omega) \tag{4.2}$$

This Fourier transform shows that the spectrum of the original signal, $\mathcal{F}X$, is replicated infinitely many times in the sampled spectrum. These replicas are spaced $\Omega = 2\pi f_s$ apart. In the case of baseband sampling, the spectrum of $x(t)$, $\mathcal{F}X$, is assumed to be 0 outside the frequency range of $[0, B]$ where B is the bandwidth of the signal defined by equation 4.3. The centre frequency, f_c of the band is defined in equation 4.4.

$$B = f_H - f_L \tag{4.3}$$

$$f_c = \frac{f_H + f_L}{2} \tag{4.4}$$

f_H and f_L are the upper and lower frequencies of the passband. Spacing of the replicas is a function of the sampling rate f_s and the center frequency f_c. These replicas are spaced $f_c \pm k f_s$ apart, where $k = 0, \pm 1, \pm 2...$ [20]. This is illustrated in figure 4.2. In this figure, two scenarios are shown. In figure 4.2 (a), the sampling rate is chosen such that the replicas are far apart from each other. In figure 4.2 (b), the choice of sampling rate does not allow for the replicas to be sufficiently separated and aliasing occurs. Reconstruction of the original signal becomes very difficult when aliasing occurs as two terms cannot be determined from their sums. Aliasing is therefore an undesirable condition. To prevent aliasing in baseband sampling applications, the sampling rate must be greater than twice the signal

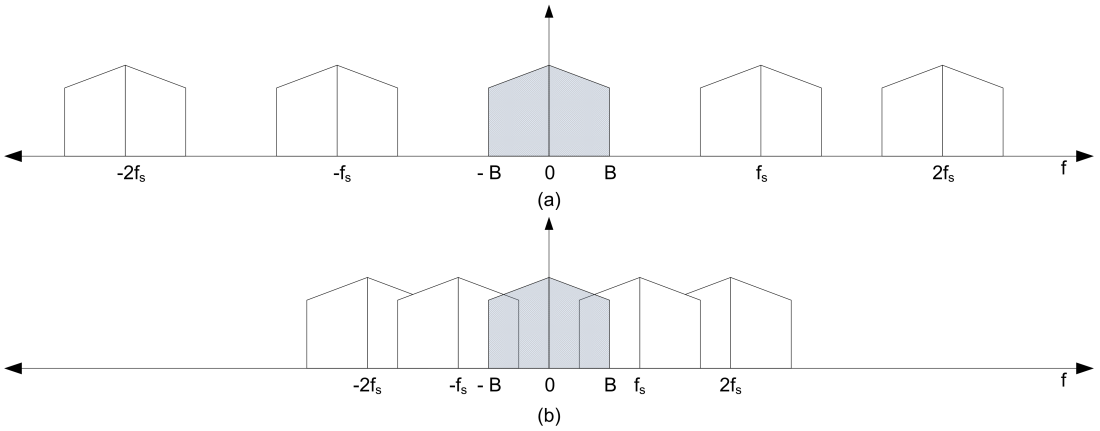

Figure 4.1: Replicas of sampled spectrum.
(a) No aliasing. (b) Aliasing

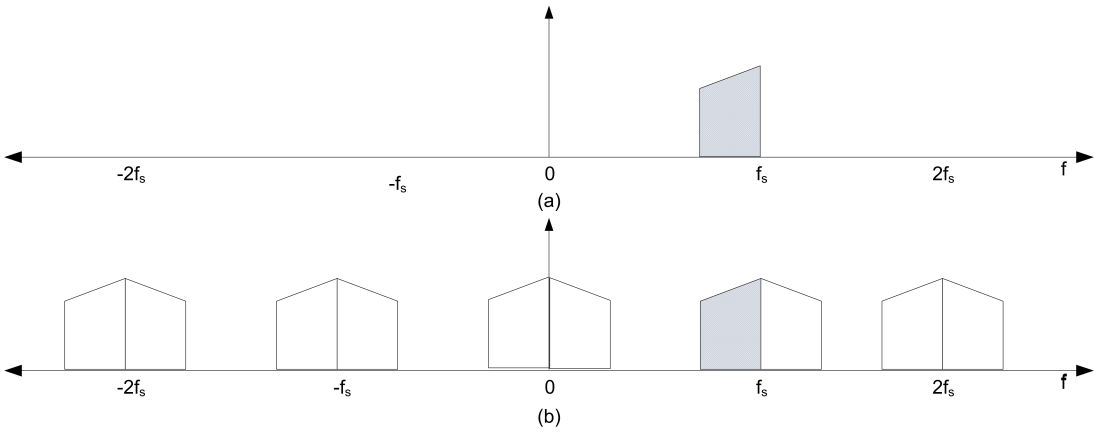

Figure 4.2: Replicas of sampled spectrum for bandpass sampling.
(a) Band limited signal. (b) Sampled signal.

bandwidth which in this case is twice the highest frequency f_H. If no aliasing occurs, the original signal can easily be reconstructed by extracting the part from $-f_s/2$ to $f_s/2$ and taking the inverse Fourier transform. Although baseband sampling is the preferred option for sampling, it often leads to impractical sampling rates.

4.1.2 Bandpass Sampling

An alternative to baseband sampling is to perform bandpass sampling where the sampling rate is chosen as a function of the bandwidth of the signal and not the upper frequency [21]. This type of sampling allows for the direct conversion of some RF band to baseband without the use of analogue downconversion. The RF signal is bandpass filtered which means that, from a theoretical view, signals outside the passband is 0. As already discussed, replications of the sampled signal will be created at integer multiples of the sample rate which includes 0 times f_s or baseband. This means that if the sample rate is appropriately chosen, a replica of the band limited signal will be positioned at baseband. This is shown in figure 4.2. In figure 4.2 (a) a band limited signal is shown to be positioned between 0 and f_s. During sampling, replicas of the original spectrum are created at multiples of f_s resulting in the spectrum shown in figure 4.2 (b) [20]. The spectrum at baseband is now inverted or flipped.

As for baseband sampling, aliasing can also occur if f_s is incorrectly chosen [22]. To prevent aliasing in bandpass sampling, the sample rate is constrained by the following equation 4.5.

$$\frac{2\,f_H}{n} \leq \frac{2\,f_L}{n-1} \tag{4.5}$$

where f_H and f_L are the upper and lower cut-off frequencies of the frequency band which is being sampled. The integer n refers to the factor by which the signal is under sampled and is constrained using equation 4.6.

$$1 \leq n \leq \lfloor \frac{f_H}{f_H - f_L} \rfloor \tag{4.6}$$

4.2 Direct Digitization Options

Based on the theory presented in section 4.1, the MeerKAT X-band band can be sampled either at full Nyquist rate, baseband sampling, or at a rate that satisfies

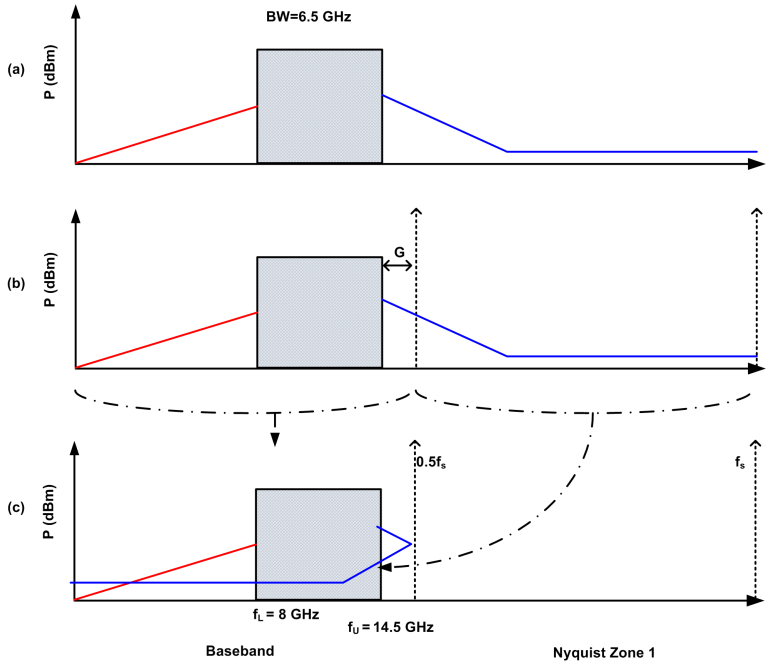

Figure 4.3: Baseband sampling of X-band.
(a) Received spectrum. (b) Sample rates and Nyquist zones overlaid. (c) Sampled spectrum. Baseband signals remain at baseband. Signals from Nyquist zone 1 flips to baseband.

the conditions for bandpass sampling. These two options will now be discussed.

4.2.1 Baseband Sampling

Based on the theory discussed for baseband sampling, the band of interest needs to be constrained such that the entire band falls in the region of $[0, 0.5\,f_s]$. This also implies that the sampling rate needs to be chosen to be $f_s \geq 2f_U$ to prevent aliasing. Since $f_U = 14.5GHz$, refer to table 3.3, the sample rate must be greater or equal to

$$f_s \geq 2f_H \geq 2 \times 14.5GHz \geq 29\,Gsps \tag{4.7}$$

Figure 4.3 illustrates the baseband sampling process for the band of interest

given the sample rate of 29Gsps. In (a) of this figure the entire spectrum up to f_s is shown. The red and the blue lines represent out of band signals. In figure (b), the sample rate f_s as well as $0.5f_s$ is shown by the dashed lines. The gap between f_U and $0.5f_s$ is shown by G and is referred to as the guard band. Note that if $f_s = 2f_U$ the guard band is zero. The spectrum of the sampled signal is shown in figure (c). Signals in the range of $[0, 0.5\, f_s]$ are replicated at baseband, while out of band signals in the range $[0.5\, f_s, f_s]$ alias to baseband and add to the signals in the range $[0, 0.5\, f_s]$. These unwanted signals can easily be removed by performing low pass filtering of the received spectrum before digitization. Baseband sampling is preferred in most applications due to the simplicity of the low pass filter as well as the resultant signal processing algorithms [20]. The problem with this method is however that there are currently no suitable commercial ADCs available that can sample at the specified rate. Another matter to consider is that the data rates which will be generated by such an ADC, if it exists, will be in the order of $87Gsps$ per polarization if a 3 bit ADC is assumed. This amount of data is very difficult to manage using current FPGA technology. For this reason this option will not be considered as part of this work.

4.2.2 Bandpass Sampling

An alternative to baseband sampling will be to perform bandpass sampling of the band of interest as discussed in section 4.1. In this method, the incoming spectrum is bandpass filtered prior to being sampled at a rate which is below the Nyquist rate. For bandpass sampling, the sample rate is constrained by the following:

$$\frac{2\, f_H}{n} \leq \frac{2\, f_L}{n-1} \tag{4.8}$$

where f_H and f_L are the upper and lower cut-off frequencies of the frequency band which is being sampled. The integer n refers to the factor by which the

signal is undersampled and is constraint using the following equation:

$$1 \leq n \leq \lfloor \frac{f_H}{f_H - f_L} \rfloor \tag{4.9}$$

Using these constraints, the under sample factor can be calculated as $n = 2$ for the specified frequency range. Since n is known, fs can also be constrained using equation 4.8, resulting in $14.5 \leq f_s \leq 16$ Gsps. Recent technology advances have been made that resulted in ADCs that can sample at these rates. One such example is a 26Gsps ADC from Analog Devices [23]. This ADC can sample up to 26Gsps and provide three output bits for each sample. Bandpass sampling is therefore a viable option which can be considered for this design, provided that 3 bits are sufficient.

This analysis has highlighted one of the main advantages of bandpass sampling. The sampling rate required to sample the same frequency range can be reduced from $29Gsps$ to approximately $15Gsps$ which also means that the data rate required has been reduced.

4.3 Disadvantages of Bandpass Sampling

The major disadvantage of bandpass sampling is that unwanted signals from all Nyquist zones aliases into the band of interests. There is no way to distinguish these unwanted signals from the wanted signals. Bandpass filtering of the complete signal chain up to the point of sampling therefore needs to be carefully considered. The way the sampled spectrum aliases when bandpass sampling is performed is shown in 4.4.

In this figure the received spectrum is shown in sub-plot (a). The band of interest is shown in green while out of band signals are shown by the red, blue and green traces. In sub-plot (b), the sample frequency, f_s, as well as $0.5f_s$, $1.5f_s$ and $2f_s$ is shown by the dashed lines. These also set the boundaries for baseband signals (0 to $0.5f_s$), Nyquist zone 1 ($0.5f_s$ to f_s), Nyquist zone 2 (f_s

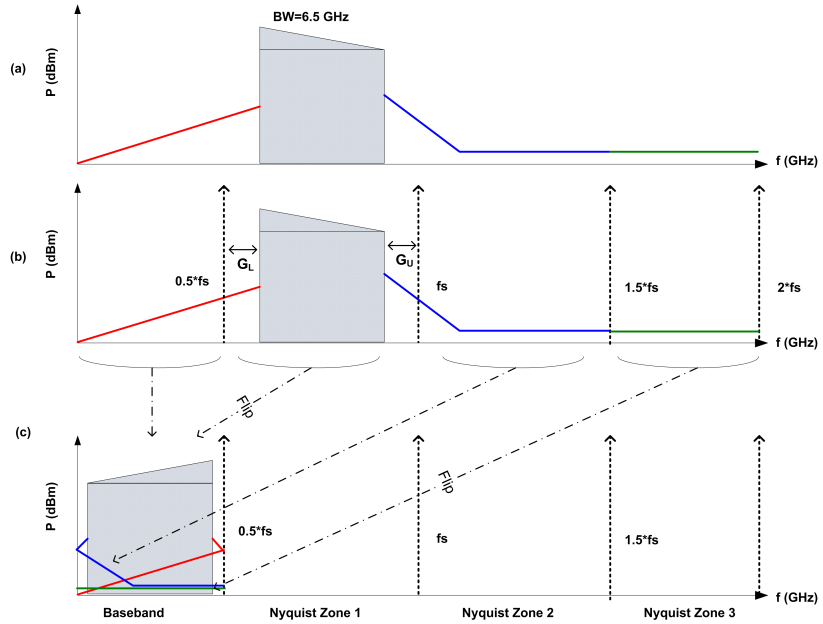

Figure 4.4: Aliasing spectrum in bandpass sampling.
(a) Received spectrum. (b) Received spectrum with sample rate and Nyquist Zones overlaid. (c) Sampled spectrum.

to $1.5f_s$) and Nyquist zone 3 ($1.5f_s$ to $2f_s$). The sampled spectrum is shown in sub-plot (c). The wanted signals located in Nyquist zone 1 is replicated at baseband where it adds to the unwanted signals at baseband. To complicate things further, unwanted signals from Nyquist zones 2 and 3 also replicated at baseband where they add to the wanted signals in the band of interest as well as the unwanted signals at baseband. This degrades the system dynamic range and efficiency [1] performance. It is clear from this diagram that strict bandpass filtering is required to remove unwanted signals at baseband as well as Nyquist zones 2 and 3 prior to sampling. This filtering is performed by an anti-aliasing filter which is discussed in the next section.

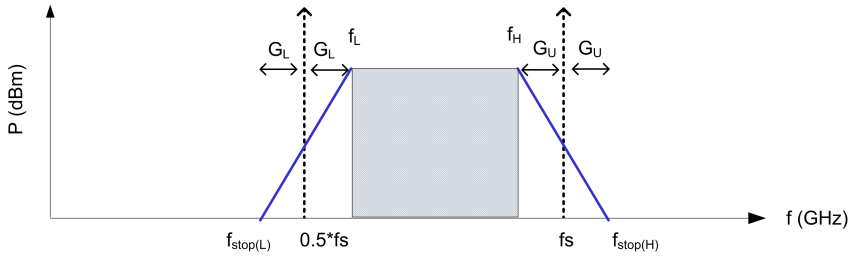

Figure 4.5: Stopband of anti-aliasing filter.

4.4 Anti-aliasing Filter

From figure 4.5 it can be seen that the upper and lower frequencies at which aliasing of signals starts is defined as follows:

$$f_{stop(L)} = f_L - 2(f_L - 0.5\, f_s) \tag{4.10}$$

$$f_{stop(H)} = f_H + 2(f_s - f_H) \tag{4.11}$$

where $f_{stop(L)}$ and $f_{stop(H)}$ are the the frequencies at which aliasing of the spectrum starts and defines the lower and upper stopband frequencies respectively. It is clear from these equations that the stopband frequencies are defined by the sampling frequency (f_s). If the sampling frequency is selected as 15GHz, the lower stopband frequency for this filter will be 7 GHz while the upper stopband frequency will be 15.5GHz. This selection of f_s results in a symmetrical filter specification as the gap between the stopband frequencies and the passband frequencies being the same at either side of the filter. A symmetrical filter roll-off is therefore achieved. If the sampling frequency is increased to 15.2Gsps, an asymmetrical filter response is required as the gap between f_H and the upper stopband frequency is larger than that of the gap between the f_L and the lower stopband frequency. The exact choice f_s can therefore be used to optimize the design of the anti-aliasing filter [24]. The filter topology suggested as part of this work leans towards a symmetrical filter implementation resulting in the sampling frequency

[1]Refers to the ratio of the output and input Signal to Noise Ratio (SNR) of the receiver

of 15Gsps being selected for this work.

The amount of stopband rejection required for this ultra-wideband receiver depends on the following:

- Signal to noise ratio requirements
- Rejection of specific out of band interfering signals such as satellite or airborne transmitters.

The analysis of these system parameters are outside the scope of this work but they are required for the specification of the filter. Specifications listed in table 3.3 states that 15 dB of rejection is required at 7 and 15GHz. In addition to these specific frequencies, 23dB of rejection is required at the point where the signals alias and a monotonic decreasing slope over the rest of the band [14]. It is important to note that any unwanted signals which is produced by the receiver itself will need to be rejected by much more to ensure that the system meets the Spurious Free Dynamic Range (SFDR) performance specification listed in table 3.3. Unwanted signals are greatly dependent on the exact implementation of the system and are therefore not discussed any further.

The specification of the filter is shown in figure 4.6 for sampling rates of 15Gsps and 15.2Gsps respectively. It is clear from this figure that the required filter response is symmetrical for a sample rate of 15Gsps and asymmetrical in the case of 15.2Gsps. The design of an anti-aliasing filter capable of these requirements is presented in chapter 6.

4.5 Simulation of Bandpass Sampling Receiver

A simulation of a direct sampling, bandpass sampling, receiver as described in prior sections was constructed using AWR software [25] and is shown in figure 4.7. In this simulation, the ADC is sampling a tone as well as noise using an 8 bit ADC.

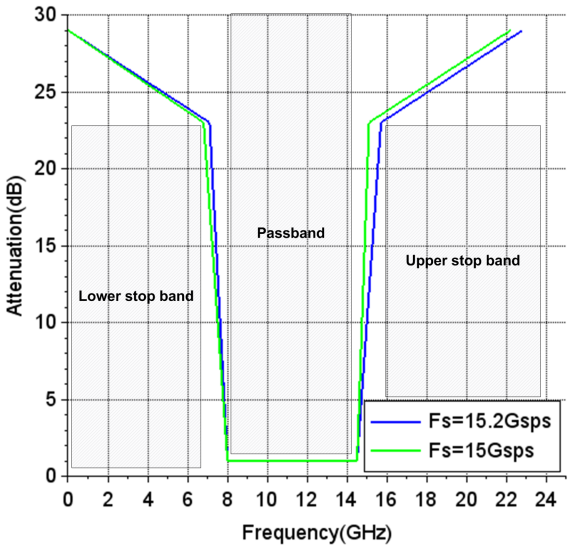

Figure 4.6: Attenuation specification of anti-aliasing filter.

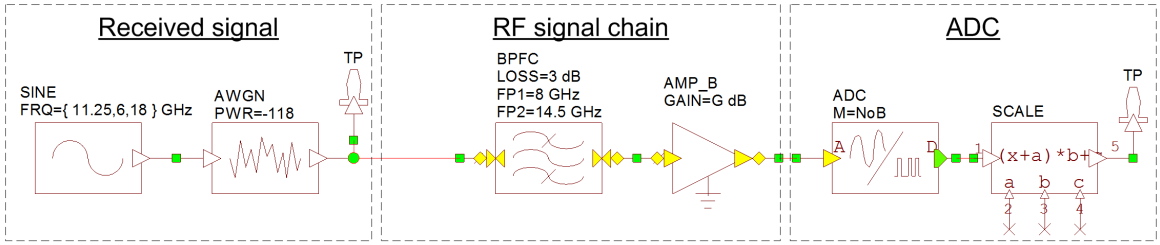

Figure 4.7: High level simulation of direct digitisation receiver.

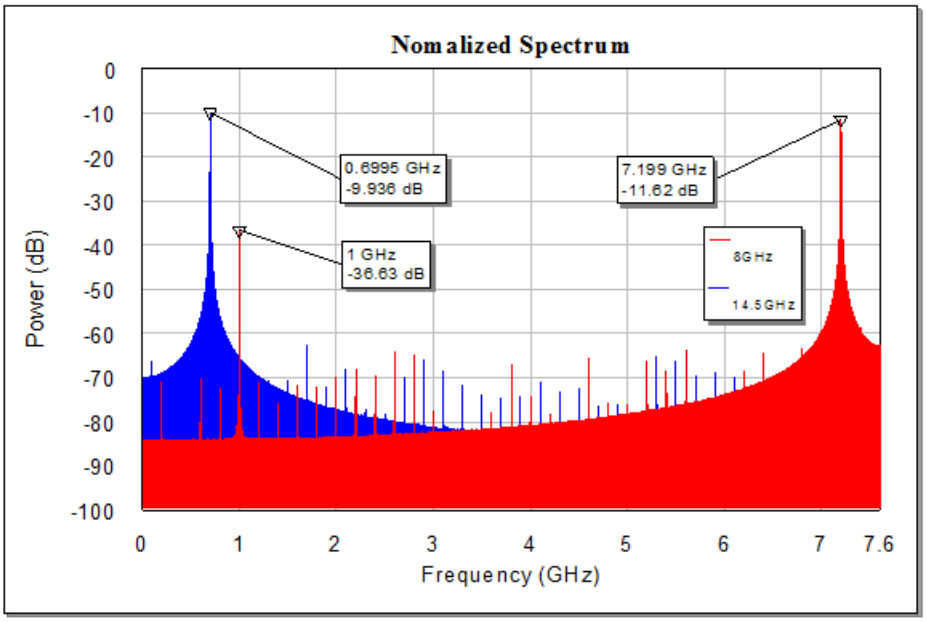

Figure 4.8: Spectrum of simulated system.
Spectrum produced with 8 (red) and 14.5 GHz (blue) signal applied. A 1 GHz interfering signal is also shown.

The sample rate is set to 15.2Gsps. The resultant spectrum is shown in figure 4.8. The blue trace shows the aliasing of the upper passband frequency (14.5GHz) to baseband while the red trace shows the aliasing of the lower stopband frequency (8GHz) to baseband. Both these frequencies alias to 700MHz and 7200MHz respectively as expected since the band is inverted at baseband. An interfering signal at 1GHz is deliberately injected inside the baseband zone at a power level of approximately 40dB below the full scale power level of the ADC. It is clear from this simulation that this interfering signal adds to the wanted signals sampled in the second Nyquist zone which explains the need to remove unwanted signals in all Nyquist zones prior to sampling. The rest of the spurious signals seen in this figure are artifacts caused by the sampling process of the ADC which cannot be changed.

4.6 Summary

In this chapter direct digitization of the X-band frequency range for MeerKAT was discussed. The theory of digitization was first presented as an introduction to this chapter. Based on this theory, two options were presented for digitization of this band namely baseband and bandpass sampling. Due to unrealistic sample rate requirements, baseband sampling was found not to be feasible for this application. Bandpass sampling was however found to be feasible and resulted in the selection of the sample rate of $f_s = 15Gsps$. This selection of sample rate also resulted in the specification of the required anti-aliasing filter which is shown in figure 4.5. Finally a simulation of a bandpass sampling receiver is presented which confirms the theory presented and design decisions taken in this chapter. In chapter 5 a heterodyne receiver architecture will be presented.

Chapter 5

Digitization using Heterodyne Receiver

In this chapter the design of a single stage heterodyne receiver is discussed. As an introduction to this chapter, the proposed signal chain of a heterodyne receiver is presented. This is followed by an theoretical overview of the mixing process. This theory is then applied to determine the key design aspects of the heterodyne receiver.

5.1 Proposed RF Signal Chain for Heterodyne Receiver

The signal chain block diagram of a heterodyne receiver is shown in figure 5.1. This block diagram shows two main sections. The first block is the front-end which is shown as a single amplifier block. The second section is the detailed block diagram of the receiver. Since the front-end is not part of the scope of work, it will only be modelled as a single amplifier stage with the specifications as given in table 3.1.

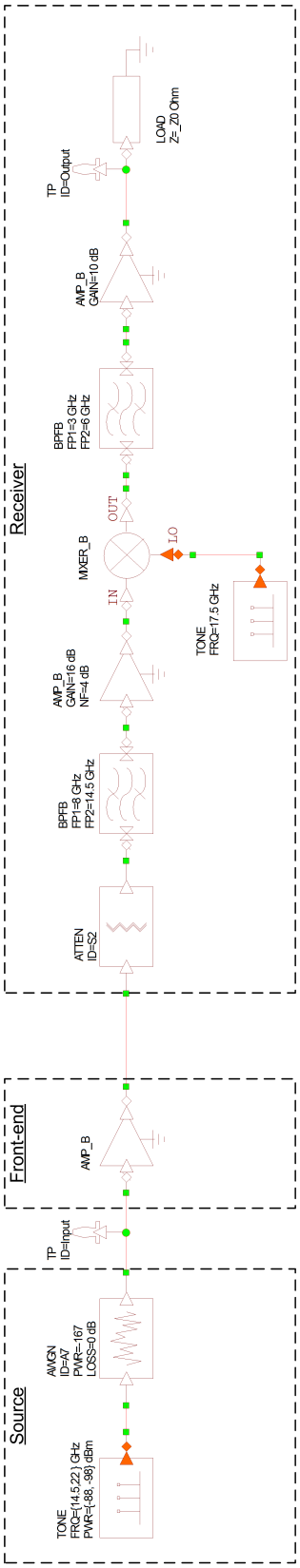

Figure 5.1: Detailed block diagram of a single channel heterodyne receiver.

The signal chain lineup of the receiver is based on a single stage heterodyne topology which consists of one mixer which down converts the specified frequency band to an Intermediate Frequency (IF). The local oscillator (LO) signal required by the mixer is provided by an internal module of the receiver. The frequency of the LO is tuned such that the correct IF is generated for the specific frequencies which are being observed. Filtering of the received signal is done using a bandpass filter with the passband being 8-14.5 GHz. A second bandpasss filter is placed on the IF port of the mixer to ensure that the mixing products of the mixer are filtered before entering the ADC. This filter also provides anti-aliasing filtering as required by the ADC. The correct signal power level into the ADC is ensured by placing amplifiers on the RF and IF ports of the mixer.

5.1.1 Mixing Process

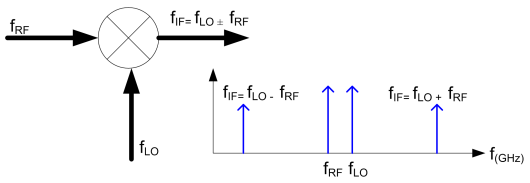

Figure 5.2: Downconversion using a mixer.

A mixer is a three port device which uses non-linear devices such as diodes to achieve frequency conversion [19]. A functional view of a mixer used for downconversion is shown in figure 5.2. The three ports of a mixer are normally designated as the RF port, Local Oscillator (LO) port and the Intermediate Frequency (IF) ports. During the downconversion process, the mixer modulates signals on the RF port with the signal applied to the LO port to produce the IF signal. The LO signal can be expressed as

$$v_{LO}(t) = cos2\pi f_{LO}\, t \tag{5.1}$$

while the RF signal can be expressed as

$$v_{RF}(t) = cos2\pi f_{RF}\, t \tag{5.2}$$

The resultant IF signal can then be mathematically expressed as

$$\begin{aligned} v_{IF}(t) &= K v_{RF}(t) v_{LO}(t) \\ &= K cos2\pi f_{RF} t cos2\pi f_{LO} t \\ &= \frac{K}{2} \left[cos2\pi \left(f_{RF} - f_{LO} \right) + cos2\pi \left(f_{RF} + f_{LO} \right) \right] \end{aligned} \tag{5.3}$$

K is a constant that relates to the conversion loss of the mixer. It is clear from equation 5.3 that the IF signal consists of the sum and difference of the RF and LO signal frequencies. Since the application is for downconversion of the RF signal, the desired IF frequency is the difference signal which can easily be selected using a low pass filter. The frequency of the IF signal, f_{IF} can be expressed in terms of the RF, f_{RF}, and LO, f_{LO}, frequencies using the following equation:

$$f_{IF} = f_{RF} - f_{LO} \tag{5.4}$$

This equation assumes that $f_{RF} > f_{LO}$. It might however be beneficial for systems designers to have allow $f_{LO} > f_{RF}$ which results in the following relationship between f_{RF}, f_{LO} and f_{IF}:

$$f_{IF} = f_{LO} - f_{RF} \tag{5.5}$$

For this work, f_{LO} is set to be above f_{RF} for reasons which will become apparent later.

Equation 5.3 provides the IF output signals from a mixer based on the multiplication of the RF and LO signals. In practice many other mixing products are produced due to the non-linear behaviour of the diodes or transistors used in the mixer. The reason being that any nonlinear device will produce not only the input frequencies but also harmonics and intermodulation products of the input frequencies applied to the device [19]. Unwanted signals produced by this nonlinear behaviour depends on the choice of f_{LO} and f_{IF} for a given f_{RF} [26].

Downconversion of a wanted RF signal is achieved by selecting the LO frequency such that the correct IF frequency is achieved and by performing filtering

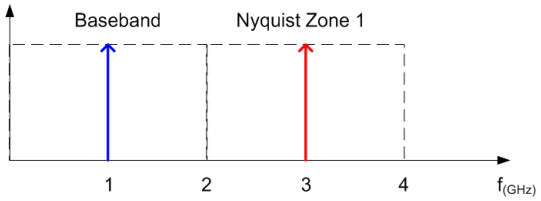

Figure 5.3: Selection of IF.

to select only the IF. The choice of the f_{IF} is constrained by the minimum instantaneous bandwidth requirement of $\geq 2GHz$ as given in table 3.3. There are two options for sampling the IF signal as already discussed in section 4.1 as part of direct digitization. The first option is to select the IF frequency such that the entire instantaneous bandwidth is at baseband. This then means that the highest frequency component of the IF signals will be 2GHz. The IF signal will then have to be sampled at $\geq 4\,GHz$ in order to satisfy the constraints of baseband sampling. The second option for sampling this down-converted signal is to select the IF such that the downconverted signal is located in the first Nyquist zone which then allows for bandpasss sampling to be performed as described in section 4.1.2. If the baseband sampling option is selected, each portion of the spectrum will have to be down converted to baseband with the IF frequency being 1GHz, shown by the blue trace in figure 5.3, which results in the frequency of the LO being

$$f_{LO} = f_{RF} + 1GHz \tag{5.6}$$

If we choose to sample in the second Nyquist zone, the IF will be selected as 3GHz, shown by the red trace in figure 5.3, which then results in f_{LO} being set to

$$f_{LO} = f_{RF} + 3GHz \tag{5.7}$$

It is clear from this, that by choosing to sample in the first Nyquist zone, the required IF frequency is much higher which result in a much greater separation between the LO and the RF signals. This is a major advantage as the greater the separation between the IF, RF and LO frequencies, the easier the filtering become which is required to get rid of unwanted mixing products [19].

5.1.2 Image Response

Another major advantage of a higher IF frequency is that the image rejection of the system can be greatly improved. There are four main signals which are produced by the mixing process namely f_{RF}, f_{LO} and the sum and differences of these to signals [19]. In this design the desired IF frequency is given by the difference between the LO and the RF signal as shown in the following equation:

$$f_{IF} = f_{LO} - f_{RF} \tag{5.8}$$

An unwanted image signal can however also appear at the IF port of the mixer. This image is as a result of the difference between the RF and LO signals. The image frequency for this application is expressed using the following equation:

$$f_{IF_{IM}} = f_{RF} - f_{LO} \tag{5.9}$$

This image signal is indistinguishable from the wanted signal which has been down converted. Signals entering the RF port of the mixer need to be appropriately filtered to ensure that the image frequencies are sufficiently rejected. Since f_{LO} is chosen to be greater than that of the RF, the LO frequency can be calculated using the following equation:

$$f_{LO} = f_{RF} + f_{IF} \tag{5.10}$$

If the receiver is set to receive the centre 2GHz band of the X-band frequency range (i.e. 10.25 to 12.25GHz) and the IF is selected to be 3GHz, f_{LO} will be set

to

$$\begin{aligned} f_{LO} &= f_{RF} + f_{IF} \\ &= \frac{10.25 + 12.25}{2} + 3 \\ &= 14.25GHz \end{aligned} \tag{5.11}$$

An image will then appear at the RF frequencies of

$$\begin{aligned} f_{IM} &= f_{LO} + f_{IF} \pm 0.5BW \\ &= 14.25 + 3 \pm 1 \\ &= 17.25 \pm 1GHz \end{aligned} \tag{5.12}$$

These signals are out of band and will therefore not have an impact provided that the band select filter provides sufficient rejection over this frequency range. If however the receiver is set to receive the lower end of the X-band frequencies (i.e. 8 to 10GHz), the image frequencies are calculated to be at $15 \pm 1GHz$. In other words, if the receiver is tuned to observe the frequency range of 8 to 10GHz, signals at 14 to 16 GHz will cause images to appear at IF which are indistinguishable from the signals which are being observed. These image frequencies cannot be removed by filtering as the lower frequency portion falls within the passband of the receiver. This is an undesirable situation which cannot be allowed. The image problem needs to be mitigated.

The options available to fix the image problem for this receiver are:

1. Increase the IF frequency

   If the IF frequency is set to be 4.5GHz the image frequencies will be at $17 \pm 1GHz$ for the low end of the X-band spectrum which is comfortably outside the MeerKAT band. This will however require an ADC which is capable of sampling at $\geq 6Gsps$ and with a RF bandwidth which will allow for the sampling of signals in the second Nyquist zone. Suitable ADCs

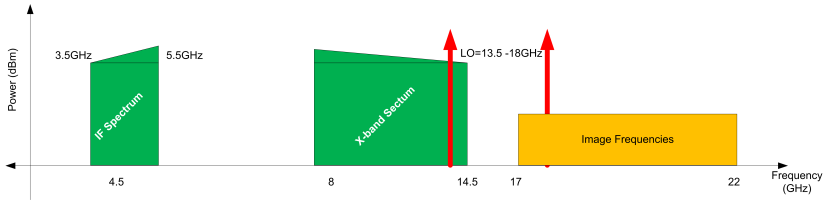

Figure 5.4: Heterodyne receiver downconversion.

from e2V [27] and Adsantec [28] have been identified that can meet these specifications.

2. Use an image reject mixer

   Image reject mixers can be used to reject the images by approximately 30dB [19]. Commercial Off The Shelf (COTS) image reject mixers capable of operating at the specified frequency ranges and bandwidths could however not be found during this investigation.

3. Dual mixing stages

   A dual mixing stage architecture can be used to firstly up convert the MeerKAT band to a very high frequency, before being mixed down again to the desired IF frequency. This design is complicated and can be difficult to achieve when considering the other system constraints such as environmental conditions and Radio Frequency Interference (RFI).

4. Use a filter bank to divide the MeerKAT band into sub-bands.

   The MeerKAT band can be divided into various sub-bands which can be selected via high frequency switches before downconversion. Each of these bands can be carefully selected such that the image frequencies are sufficiently rejected. The disadvantage of this option is that the signal path up to the mixer will have to be duplicated. In addition to this many complicated filters will need to be designed to select these sub-bands. This option will significantly increase the cost of the system.

The most feasible option from the list given above is to increase the IF frequency to 4.5GHz. The downconversion process described above is illustrated in

figure 5.4. In this figure, the band of interest is indicated between 8 and 14.5 GHz, the IF frequency is $4.5 \pm 1GHz$ and the image frequencies are shown in yellow. The LO frequency range is shown by the red functions. These indicate the tuning range required by the LO which is between 13.5 and 17GHz. The IF signals will be bandpass sampled. This means that the sampling rate is bound by equations 4.5 and 4.6 as was discussed in section 4.1.2. Using these equations, the under sampling factor n is calculated as 2 and the sampling frequency range as $5.5 \geq f_s \geq 7$ Gsps. A similar analysis as was done in section 4.4 can be done to determine the anti-aliasing filter requirements for the IF signal. This analysis is however outside the scope of this report.

5.2 Filter Rejection

One major advantage of the single stage heterodyne architecture compared to that of the direct digitization architecture is that the out of band rejection required by the filter is different for the upper band compared to that of the lower band. Since the heterodyne receiver can be tuned to select only the band of interest, the main concern would be the rejection of the image frequencies. From table 3.3, out of band rejection is specified as 15dB at 7 and 15 GHz. These specifications are however not that important for this architecture since the LO can be set such that these signals are not selected. These signals also do not correspond to any of the image frequencies that need to be rejected.

The main aim of the band select filter is therefore to reject the image frequencies. As already mentioned, signals at the image frequencies will be indistinguishable from the wanted signals which are in-band. Interfering signals at the image frequencies will therefore degrade the overall system Spurious Free Dynamic Range (SFDR) [1] performance which is specified in table 3.3 as 55dB. The band select filter therefore needs to provide 55dB of rejection of the image frequencies.

[1] Power ratio of the fundamental signal to the strongest spurious signal in the output of the ADC

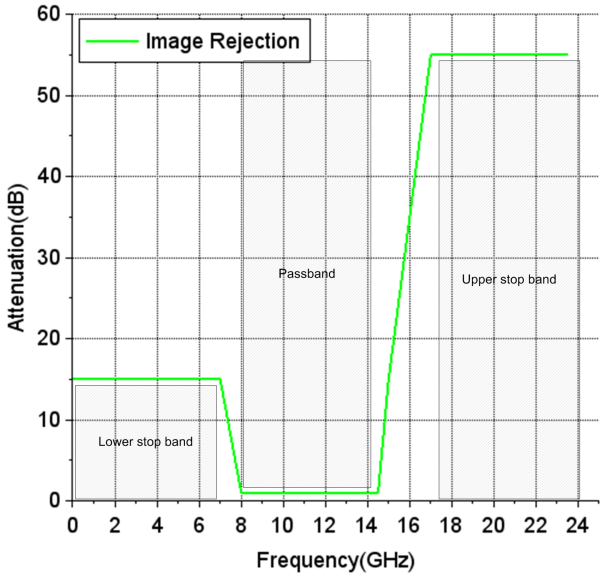

Figure 5.5: Image reject filter attenuation for heterodyne receiver.

5.3 Band Select Specification

Based on the analysis above, the detailed specifications of the single stage heterodyne receiver is given in table 5.1.

Table 5.1: Detailed specifications of heterodyne receiver.

Parameter	Specification
RF Frequency range	8-14.5 GHz
IF Frequency	4.5 GHz
IF Bandwidth	2.5 GHz
LO Frequency	RF+IF
Image frequencies	17-23.5 GHz
Image rejection	55 dB
Stopband frequencies	7 and 15 GHz
Stopband rejection	15 dB

The frequency response of the band select filter, which is actually an image reject filter, is shown in figure 5.5. The detail design of a filter capable of this frequency response is described in chapter 6.

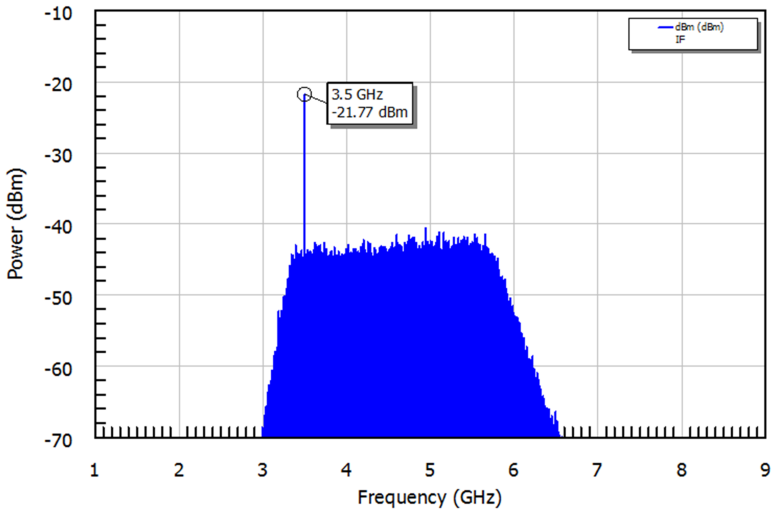

Figure 5.6: Simulated spectrum of heterodyne receiver.

5.4 System Simulation

A simulation of the proposed heterodyne receiver shown in figure 5.1 was performed using AWR software [25]. The resultant IF spectrum is shown in figure 5.6. The LO was set to 18GHz. This selects the upper portion of the band for this simulation. A signal was injected at the input of the front-end at a frequency of 14.5GHz with a power level of -88dBm. The resultant spectrum shows that the 14.5GHz tone mix down to an IF frequency of 3.5GHz as expected. Similar test was done for a tone of frequency of 8GHz with the LO set to 13.5GHz. In this case the tone mixes to an IF frequency of 5.5GHz as expected. The resultant spectrum in 5.6 also shows that no unwanted mixing products are observed in the downconverted spectrum.

5.5 Summary

In this chapter the design of a single stage heterodyne receiver capable of meeting the requirements of the MeerKAT X-band was presented. As an introduction to this chapter, the theory of the mixing process was presented. This theory was

then used to make key system design choices such as the selection of the LO and IF frequencies. The first selection of the IF frequency resulted in an unwanted image being created at the IF of signals located in the upper part of the band when the receiver was tuned to receive the lower portion of the band. This was mitigated by increasing the IF frequency. The specification of the image reject filter required by this receiver was derived based on the selection of the IF and LO frequencies. Finally a signal path simulation of the heterodyne receiver was presented to confirm that the design perform as expected. The detailed specification of the receiver is listed in table 5.1 and the required frequency response of the image reject filter is shown in figure 5.5. In the next chapter a filter design is presented which can achieve the specification of this image reject filter.

Chapter 6

Design of Band Select Filter.

In this chapter a bandpass filter is designed to cater for the requirements of a X-band single stage heterodyne receiver as discussed in chapter 5. However as a design goal, the filter will also be designed to achieve the specifications of the anti-aliasing filter required for the direct digitisation design with a sample rate of 15GHz as described in chapter 4. The attenuation as a function of frequency response of the two types of filters required for these designs are shown on the same plot in figure 6.1. The complete list of specifcations for the filter is given in table 6.1 as has been derived in the previous chapters.

6.1 Choice of Filter

The fractional bandwidth required of a bandpass filter capable of meeting the passband specification can be calculated using the following equation:

$$BW_{\%} = 100 \times \frac{f_u - f_L}{\sqrt{f_u \times f_L}} \tag{6.1}$$

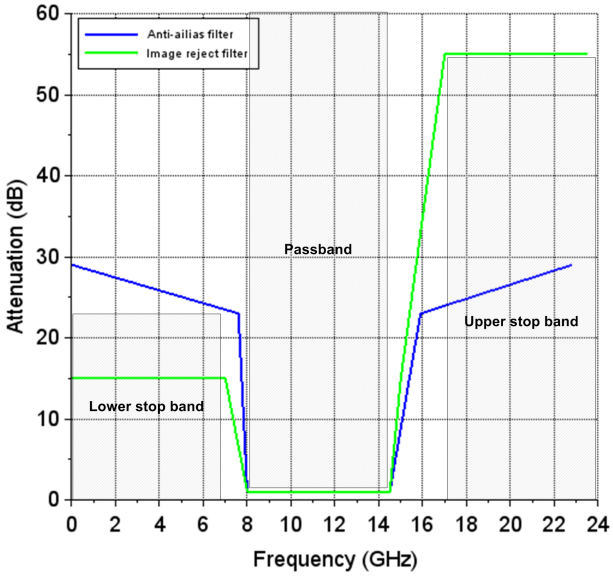

Figure 6.1: Combined minimum filter attenuation specifications.

Table 6.1: Band select filter specifications.

Parameter	Specification
Passband	8-14.5GHz
Lower stopband frequency	7GHz
Upper stopband frequency	15GHz
Stopband attenuation	15dB
Image band	17-22GHz
Image band rejection	$\geq 55dB$
Lower aliasing band	0-7GHz
Upper aliasing band	15.5 - 22.5GHz
Aliasing band rejection	$\geq 23dB$
Returnloss	$\geq 10dB$
Insertion loss	$\leq 1.5dB$
Passband ripple	$\leq 1dB_{pk-pk}$
Groupdelay flatness	$\leq 3.5ns$

Where f_U and f_L are the upper and lower passband frequencies. For the MeerKAT filter, this is calculated to be 60.4 %. Filters with fractional bandwidths of $\geq$ 20% and bandwidth exceeding 500MHz is classed as ultra-wideband [29] filters which limits the type of filter topology which can be used to implement

these types of filters. Two filter topologies were identified as possible solutions and investigated as part of this work. These will now be discussed.

6.1.1 Cascaded Low-pass and High-pass Filters

Cascading of filters have been shown to be a very good implementation choice to realize ultra-wideband filters [30; 31].Frequency responses can be achieved by cascading, low-pass and high-pass filters, high-pass filters and band-stop filters or low-pass filters and band-stop filters depending on the specification that needs to be achieved. The main advantage of cascading filters is that the lower and upper stopband can be independently designed which is very useful in designs where asymmetrical filter responses are required as is the case for for the image reject filter of the heterodyne receiver of MeerKAT. High-pass and low-pass filters are typically cascaded in ultra-wideband applications as these filters typically provide very wide passband responses. The disadvantage however is that these filters can take up significant amount of space and impedance mismatch between the filters can result in undesirable ripple in the passband.

Quasi-lumped element designs implemented on Suspended Strip Line (SSL) has been shown to be a good option when designing cascaded low pass and high pass filters [32]. SSL is a special form of strip line structure where the substrate is suspended in air and enclosed by metal on all sides similar to a waveguide as shown in figure 6.2. The advantage of this structure is that the modes of propagation of the signal through this structure is purely Transverse Electromagnetic (TEM) which means that the electric and magnetic fields of the signal are orthogonal to each other and orthogonal to the direction of propagation [19]. This yields a major advantage of this type of structure above micro-strip structures in that there is no dispersion [1] of the signals propagating through the structure. Design equations for the calculation of the impedance and effective dielectric constant of transmission lines implemented in SSL is given in appendix A 8.2.

[1]Refers distortion of a signal due to a frequency dependency of the phase velocity of a signal traveling on a dielectric medium [19].

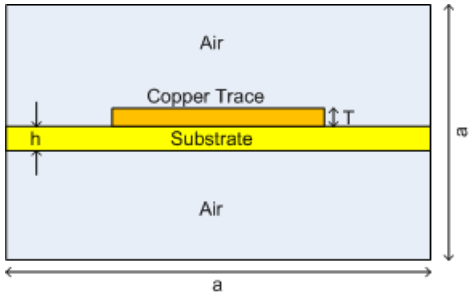

Figure 6.2: Suspended Strip Line (SSL) structure.

SSL structures are ideally suited for the implementation of quasi-lumped element capacitors and inductors since both sides of the substrate can be used [32]. Series inductors can be implemented using thin traces of transmission lines which can be connected in series or it can be connected to ground to realize shunt inductors as shown in figure 6.3. Series capacitors can be realized by small gaps in the transmission line or by placing metal patches on opposing sides of the substrate to implement Metal Insulating Metal (MIM) capacitors [18]. Shunt capacitors to ground can also be realized using MIM capacitors by connecting the one side of the capacitor to ground as shown in figure 6.4. The typical inductance and capacitance which can be practically realized using these structures are shown in figures 6.5 and 6.6.

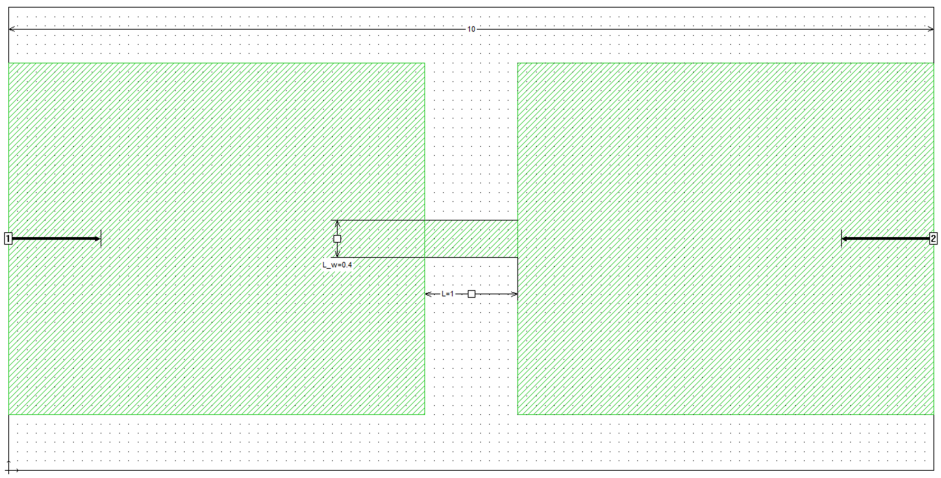

Figure 6.3: SSL series inductor.

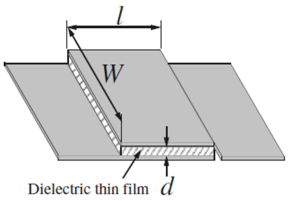

Figure 6.4: SSL MIM capacitor.

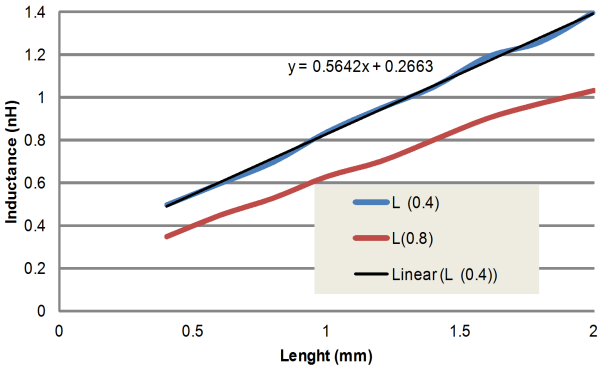

Figure 6.5: SSL series inductance as a function of transmission line length. *Inductance for 0.4 mm and 0.8 mm transmission line widths shown in blue and red respectively. Equation provides a linear approximation of the 0.4 mm transmission line.*

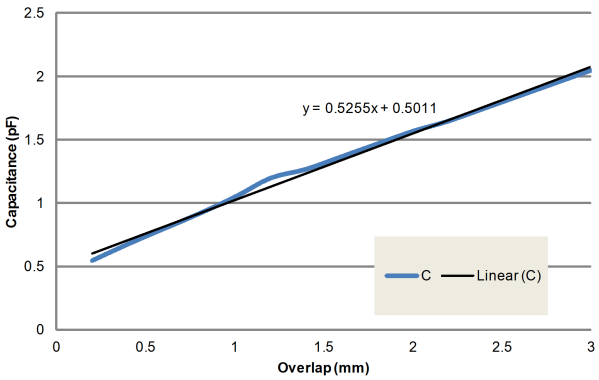

Figure 6.6: SSL MIM capacitance value as a function of overlap. *Equation provides a linear approximation of capacitance vs. overlap.*

Using AWR software [25], an estimation of the lumped element component values required to realize an 11th order low-pass and high-pass filter with a type 1

general Chybychev response can be made. For this design inductor values required for the low-pass filter is in the range of 0.14 to 0.8 nH while the capacitance required is approximately 0.1pF. For the high-pass filter, the inductance required is 1.1 to 2 nH while the capacitance required being 0.25 to 1.5pF. It is clear that the range of values required are mostly outside the range of values shown in figures 6.5 and 6.6.

The problem with realizing small value of inductance and capacitance is that parasitic capacitance between these components and the metal structure tends to dominate. This prevents the implementation of these very small value components. Due to these limitations, this filter design is found not to be suitable for this application. Quasi-lumped element filters implemented on SSL is however an implementation option which can be used for the design of the IF filter required for the heterodyne receiver and will be considered for future work.

6.1.2 Distributed Band-pass Filter

Another filter topology that can be used for wide band applications is a distributed band-pass filter. This type of filter has been shown to be ideally suited for ultra-wideband applications [18; 33; 34]. In [33] an ultra-wideband filter with an fractional bandwidth of 69 % and center frequency of 4.5GHz was demonstrated.

A distributed band-pass filter uses shunt quarter wavelength ($\lambda_0/4$) short-circuited stubs to implement the required filter element values which are also separated by $\lambda_0/4$ connecting lines [18]. A variant on this filter is an optimum distributed high-pass filter [18] which also deploys short circuit stubs, but these stubs are not $\lambda_0/4$ stubs, but rather stubs with length of θ_c at the cut-off frequency of the high-pass filter. This high-pass filter has a pass-band from θ_c to $\pi - \theta_c$. The pass-band repeats periodically at $\theta = \frac{3\pi}{2}, \frac{5\pi}{2}...$ and has attenuation poles at $\theta = \pi, 2\pi....$ The value of θ_c can be calculated for a specified pass-band using the following equation:

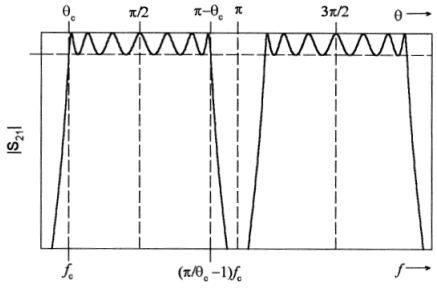

Figure 6.7: Frequency response of optimum distributed filter.

$$\theta_c = \frac{\pi\, f_L}{f_u + f_L} \tag{6.2}$$

Where f_L and f_u is the upper and lower passband frequency of the filter. Using this equation, θ_c is calculated as 64° for the MeerKAT passband. The frequency response of this type of filter is shown in figure 6.7 [18].

6.2 Design of Distributed Bandpass Filter

The schematic of an 11th order distributed bandpass filter is shown in figure 6.8. The impedance and lengths of each of the transmission lines are determined using [25] based on the lower and upper stopband frequencies, filter order and θ_c as calculated in equation 6.2.

In this design the electrical lengths of the transmission lines was selected to be approximately 64° and subsequently optimized to approximately 63°. The impedance of each of the transmission lines are shown in table 6.2.

The simulated results of the ideal implementation of this filter is shown in figure 6.9.

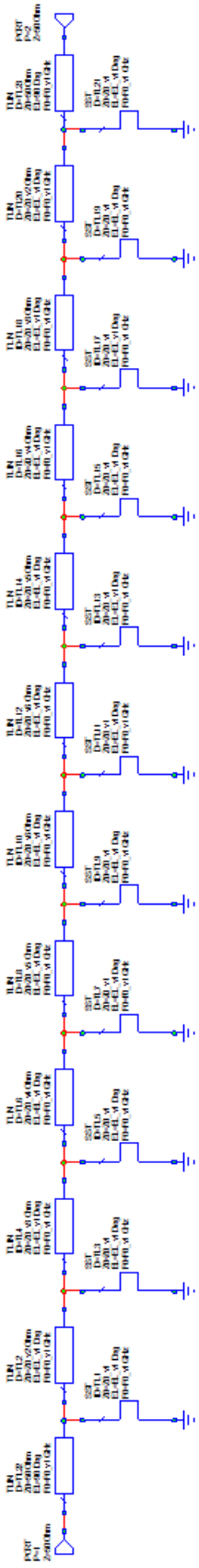

Figure 6.8: Transmission line schematic of distributed filter.

Table 6.2: Optimized impedance values.

Transmision line	Impedance
Shunt transmission lines	35.9 Ω
TL2 and TL20	52 Ω
TL4 and TL18	65.4 Ω
TL6 and TL16	74.2 Ω
TL8 and TL14	78.2 Ω
TL10 and TL12	79.2 Ω

6.3 Realization of Filter

This filter is to be integrated with other discrete components such as amplifiers, mixers and attenuators. All of these components are typically designed for micro-strip designs. For this reason the design is chosen to be implemented on micro-strip as this will ease the integration with the rest of the circuit. This decision might however result in higher insertion loss which can be mitigated by increasing the overall gain of the receiver to compensate for the additional loss. This additional loss will not have an impact on the overall noise performance of the system as shown in section 3.2.2.2.

The Mercurywave 9350 [35] substrate was selected due to a dielectric constant of 3.5 and low dissipation factor. This material is readily available from local suppliers and is available in various substrate thicknesses.

The substrate height was chosen as 211 micrometre (μm) which ensures that the trace thicknesses of the transmission lines given in table 6.2 does not violate the minimum trace thickness specification which the manufacturer can accommodate. In this case the minimum trace width is $125\mu m$. All traces must therefore be $\geq 125\mu m$ and preferably $\geq 200\mu m$.

The widths and lengths of the transmission lines are then calculated for micro-strip lines on the selected substrate. The calculation of the widths and lengths are described in detail in [18; 19]. Many calculators have also been developed for this purpose such as the one by AWR [25] which was used in this work.

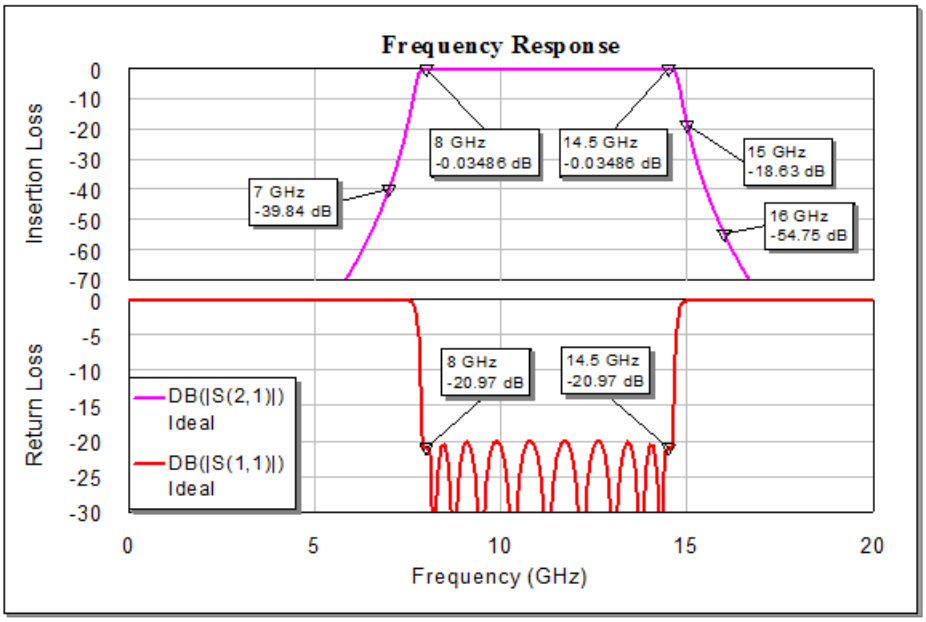

Figure 6.9: Frequency response of ideal distributed filter.

The last thing to consider is the connection of the shunt transmission lines to ground. This is done by connecting the transmission line on top of the substrate to the ground plane at the bottom of the substrate using a via. By inserting the via, additional inductance is added to the end of the transmission line. This needs to be compensated for as this additional inductance will change the frequency response of the filter.

The widths and lengths of each of the transmission lines of this filter are given in table 6.3 after optimization and compensation for the addition of the vias. A schematic of the distributed filter, converted to a micro-strip design and including the vias is shown in figure 6.10. The lengths of the shunt transmission lines have been optimized to compensate for the additional inductance of the vias to ground. A physical view of the filter is shown in figure 6.11.

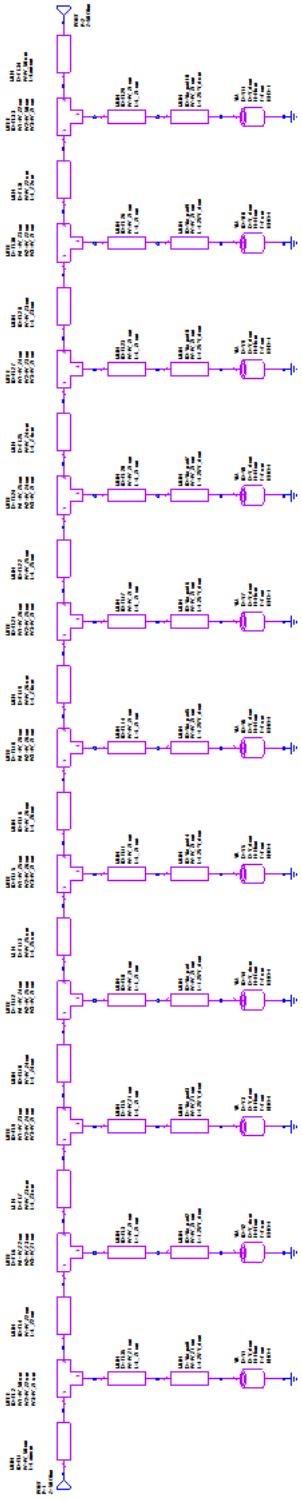

Figure 6.10: Transmission line schematic of distributed filter including vias.

Table 6.3: Physical dimensions of transmission lines.

Transmision line	Width (μm)	Lenght (μm)
Shunt transmission lines	660	3586
TL2 and TL20	425	4064
TL4 and TL18	275	4064
TL6 and TL16	196	3927
TL8 and TL14	174	4126
TL10 and TL12	153	4312

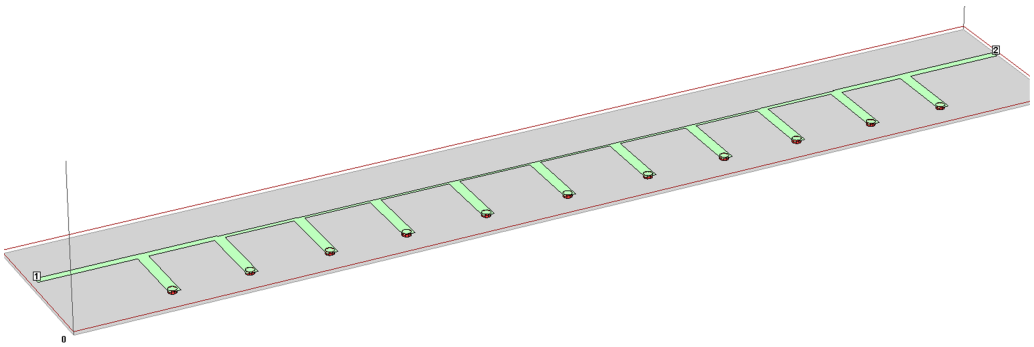

Figure 6.11: Physical view of distributed filter.

6.4 Simulated results

The physical implementation of the filter is then simulated using a much more accurate Electro-Magnetic (EM) simulator. This type of simulator simulates the electro-magnetic propagation of signals through the physical structure. It is therefore able to simulate a near real world performance of the filter.

Two EM simulators were used in this design. The first being Axiem EM simulator from AWR [25] and the second being the SONNET EM simulator [36]. The comparison of the simulations are shown in figure 6.12. It can be seen that there is practically no difference between the EM simulations with respect to the insertion loss. The reason for the discontinuity in at approximately 15.6GHz in the SONNET simulation is not known.

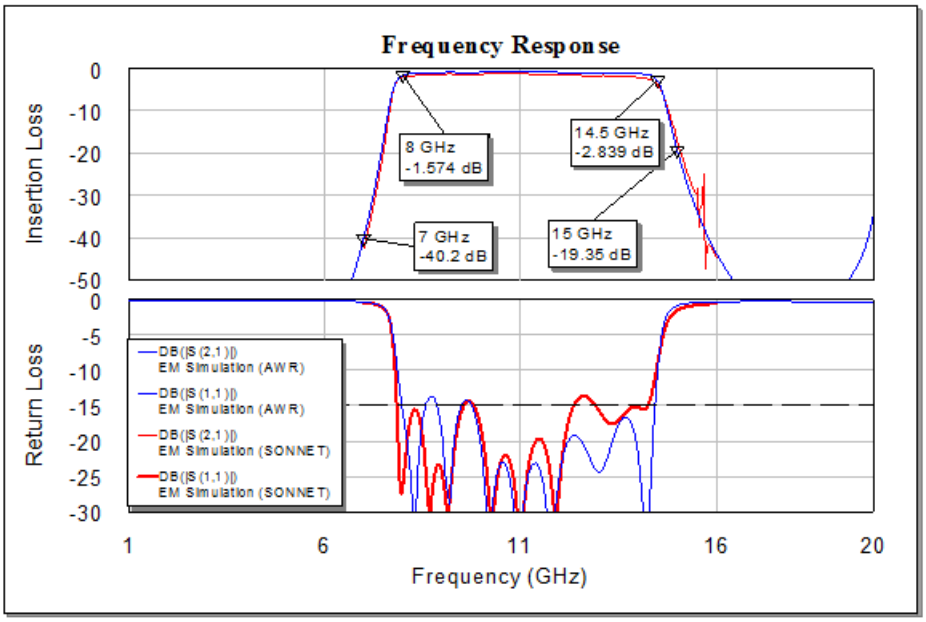

Figure 6.12: EM simulated frequency response of the filter.

6.5 Measured results

A photo of the constructed filter is shown in figure 6.13. Due to their availability, SubMiniature version A (SMA) connectors are mounted on the input and output of the filter to enable the testing of the filter by means of a network analyzer. The measured insertion and return loss of the filter is shown in figure 6.14.

The return loss of the constructed filter is less than the specified value of -10dB. This is due to the effect of the connectors which have not been removed from these measurements. This can be done by designing an appropriate Thru Reflect Line (TRL) calibration which include the connectors. The final design will not use connectors. This aspect will be improved on during next design iterations of the filter. The repeat response of the filter at 21.4GHz is expected as the transmission lines becomes half a wavelength at double the frequency. Although this is inside the image frequency range of the filter it will be attenuated by the

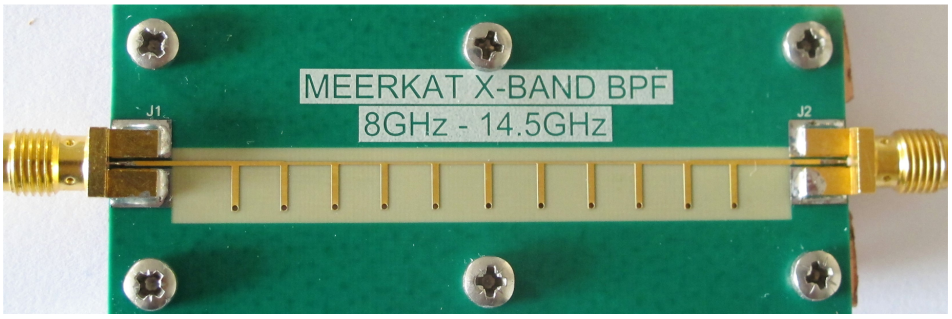

Figure 6.13: Constructed filter.

frequency limitation of other components such as the amplifiers and the mixer and is therefore not a concern in this design. The measured group delay performance of the filters are shown in figure 6.15. It is clear that the group delay variation of the filter is much less than 3.5ns as specified.

A comparison between the measured frequency response and the specification is shown in figure 6.16. It is clear from this figure that the distributed filter meets the stopband specification for the anti-aliasing filter. Additional suppression is however required in order to provide the required image rejection above 18GHz. This rejection can be provided by other components in the line-up such as the mixer as will be discussed in chapter 7. The passband frequency of the filter is correct, but the insertion loss exceeds specification.

6.6 SSL implementation of Distributed filter

Although the micro-strip filter designed in the previous section meets all the specifications, the widths of the transmission lines are of concern. PCB manufacturing tolerances can result in variation of trace widths which can result in variation in frequency response between manufacturing batches. This can be prevented by having wider traces which are less sensitive to manufacturing tolerances. In order to increase trace widths, the distributed filter described above can be constructed using SSL. Trace widths will be greatly increased from that used in the micro-strip design. A SSL design will also improve insertionloss of

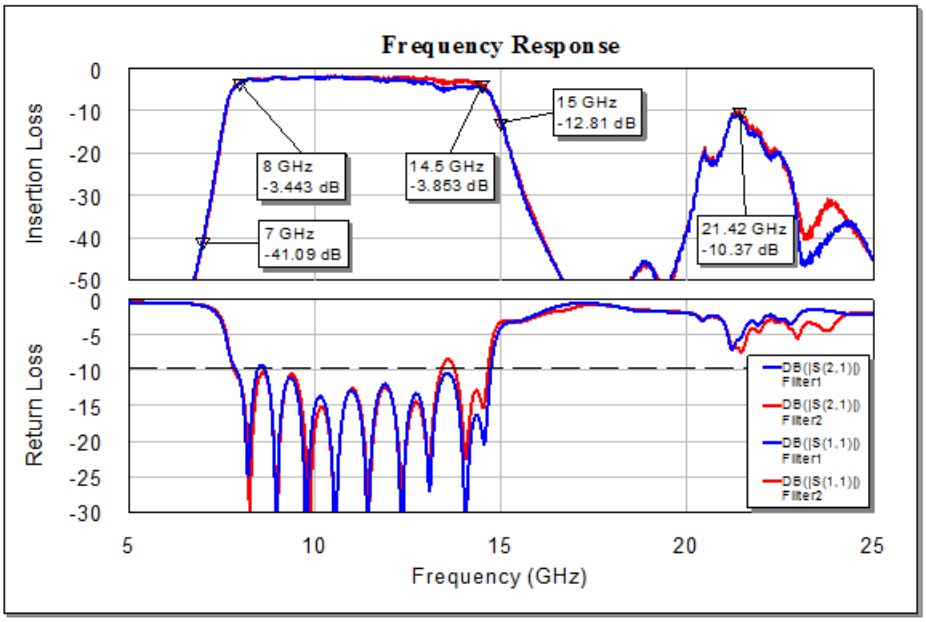

Figure 6.14: Measured frequency response of the filter.

the filter in the passband [31]. From figures 2 and 3 in appendix A (8.2), the impedance of a SSL trace of width x can be can be calculated using the following equation:

$$Z = 170.03\, e^{-0.342\, x} \tag{6.3}$$

Solving this equation for x results in the following equation which allows for the calculation of the trace width (x) that yields a specified impedance, Z:

$$x = -\frac{ln\,(Z/170)}{170.03} \tag{6.4}$$

Using this equation, the trace width for the various impedances required by the distributed filter can now be calculated. The results are shown in table 6.4.

The length of the connecting transmission lines as well as the shunt stubs is required to be $\Theta_c = 63°$ as discussed in section 6.2. The guided wavelength λ_g of

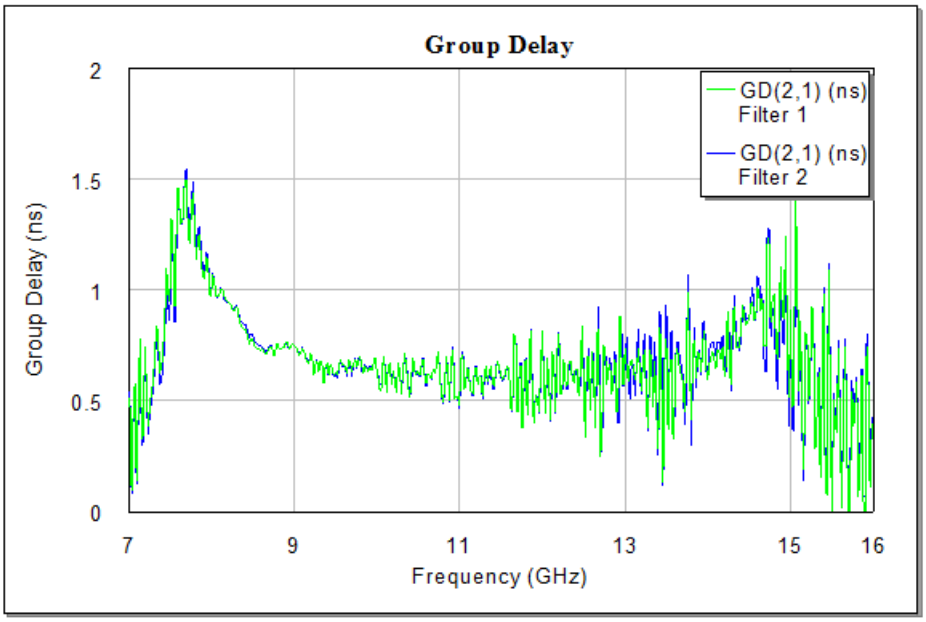

Figure 6.15: Measured group delay response of the filter.

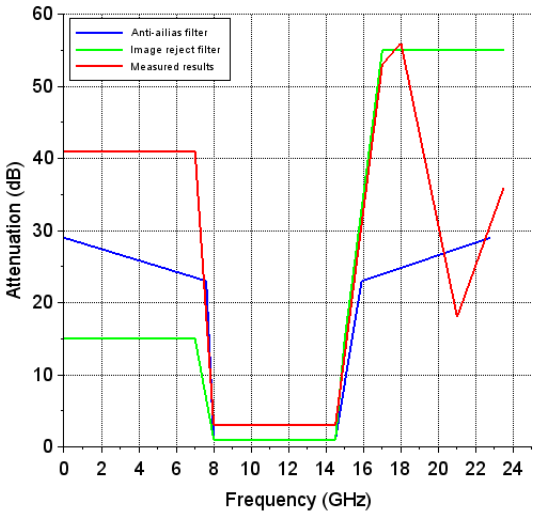

Figure 6.16: Comparison of specification and measured results.

Table 6.4: SSL trace width for specified impedance.

Transmision line	Impedance	Width (mm)
Shunt transmission lines	35.9 Ω	4.52
TL2 and TL20	52 Ω	3.44
TL4 and TL18	65.4 Ω	2.78
TL6 and TL16	74.2 Ω	2.41
TL8 and TL14	78.2 Ω	2.26
TL10 and TL12	79.2 Ω	2.22

a wave propagating in SSL can be calculated using equation 6.5.

$$\lambda_g = \frac{c}{f\sqrt{e_r}} \tag{6.5}$$

where $c = 300 \times 10^6 ms^{-1}$ which refers to the speed of light. The frequency $f = f_L = 8GHz$ as defined in section 6.2. The effective dielectric constant of a SSL structure is shown in figure 3 in appendix A (8.2) and is taken to be $e_r = 1.26$. Using these values, the guided wavelength can be calculated as $\lambda_g = 33.4\,mm$. A phase shift of 63° can therefore be achieved using a transmission line with a length of

$$T_{length} = \lambda_g \frac{\Theta_c}{360} = 5.85mm \tag{6.6}$$

Using the widths of the various transmission lines given in table 6.4 as well as the stub and transmission line length T_{length} the ideal filter shown in figure 6.8 can be physically realized on SSL. The physical layout of the transmission lines is shown in figure 6.17. These transmission lines are implemented on the same substrate used for the micro-strip design i.e. $211\mu m$ thick substrate Mercurywave 9350 substrate [35].

The substrate is mechanically mounted in an aluminum enclosure which suspends the substrate in air such that the structure shown in figure 6.2 is realized. This is shown in figure 6.18. In this figure, the blue structure represents an air gap. The open space around the filter structure is modeled as a Perfect Electrical Conductor (PEC) which is connected to ground. The stubs are also suspended in

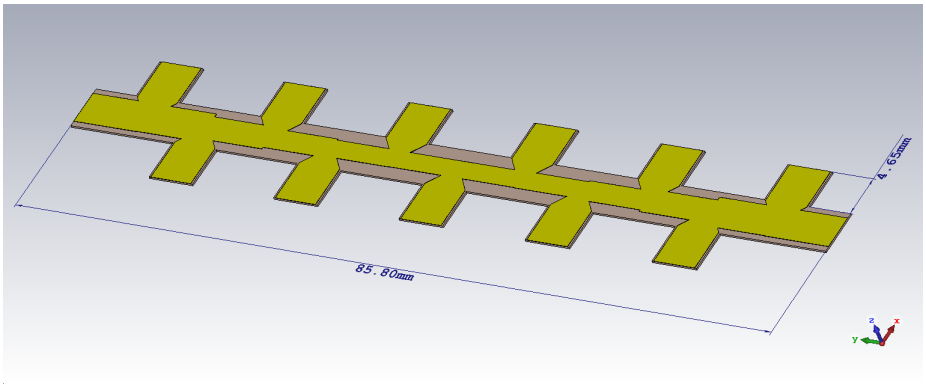

Figure 6.17: PCB of distributed filter implemented on SSL.

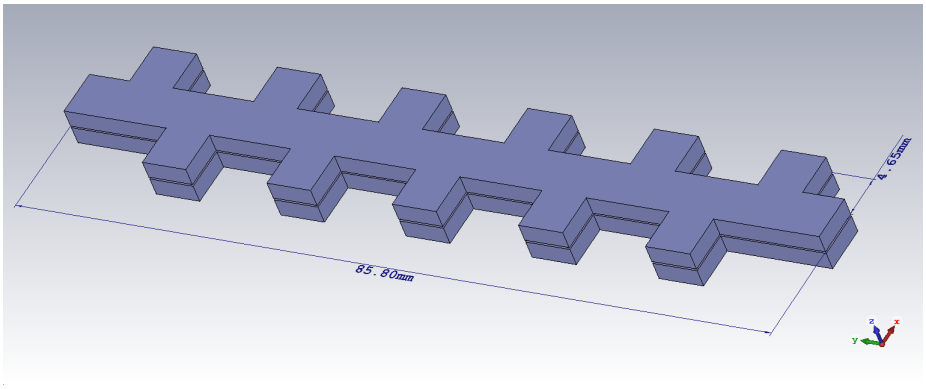

Figure 6.18: Distributed filter implemented on SSL.

air. Shunt stubs are short circuited to the edge of the structure which is connected to ground.

A model of this filter was constructed using CST [37] which is a 3D electromagnetic simulation software. Optimization of the transmission line widths listed in table 6.4 as well T_{length} was required to achieve the desired frequency response. The maximum optimization required for the line widths was 8% of the theoretical value. After optimization, T_{length} was 22% longer than the calculated value. This increase in length of T_{length} is due to the additional length which gets added to the transmission lines as a result of the very wide traces used required by the series transmission lines. The simulated insertionloss and returnloss response of this filter is shown in figure 6.19 and 6.20 respectively. Very low , $\leq 1\,dB$, insertionloss is achieved within the passband of the filter which lies between 8 -14.5GHz. Out

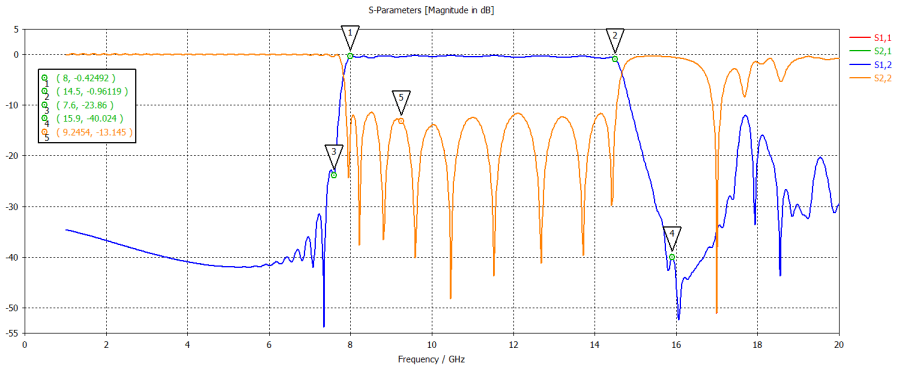

Figure 6.19: Distributed filter S-parameters.

of band rejection at 7.6 and 15.9 GHz is $\geq 23\,dB$ which meets the specification for anti-alias filtering. Out of band rejection above 17GHz does however not meet specification. This is due to an unwanted increase in S21 response above 16GHz which is also coupled to a very narrow dip in S11 at approximately 17GHz. The cause of this is not known at this stage and will be investigated in future work. Over the passband frequency the returnloss, S_{11} is $\leq -13\,dB$. The groupdelay of the filter is maximum $1.3\,ns$ over the passband of the filter as shown in figure 6.20 which is less than the specified value of 3.5ns.

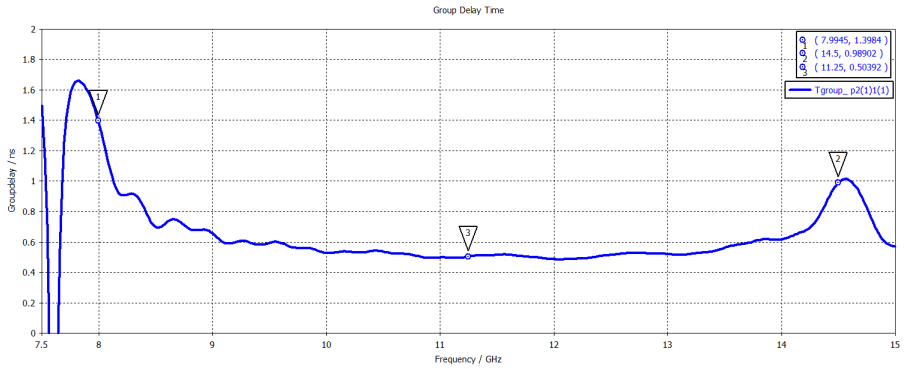

Figure 6.20: Distributed filter group delay.

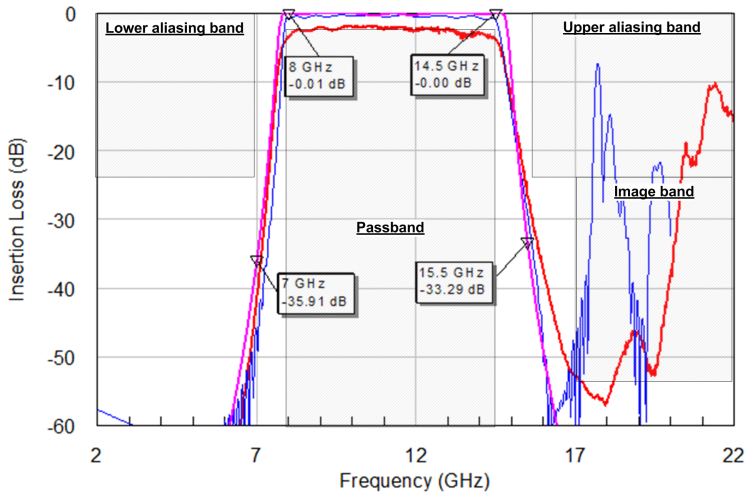

Figure 6.21: Comparison between SSL and Micro-strip implementation. *Ideal distributed filter (pink trace). Disrtibuted filter implemented on micro-strip (red trace). Distributed filter implemented on SSL (blue trace)*

6.7 Comparison of SSL and Micro-strip designs

In figure 6.21, the S_{21} response of an ideal distributed bandpass filter, pink trace, is compared to that of a distributed filter implemented on micro-strip, red trace, and a distributed filter implemented on SSL, blue trace. The results for the micro-strip implementation is based on measurements, while the ideal and SSL results are simulation based. The passband, upper and lower aliasing bands as well as the image band are idicated by the shaded areas on this plot. The filter response is not permitted to enter these areas. The passband insertion loss of the simulated SSL filter is very close to that of the ideal filter whereas the micro-strip filter adds approximately 2dB insertion loss in the passband. Both the micro-strip and the SSL filter comfortably meets the rejection required for the upper and lower aliasing bands given the specification of 23dB. The SSL filter does however approximate the ideal filter better than the micro-strip filter up to approximately 16GHz. An unwanted decrease in the stopband attenuation is produced by the SSL filter at approximately 18GHz resulting in insufficient rejection in the image band. The cause of this decrease is not known at this stage and will be investigated in future designs. The micro-strip filter meets the

specification of 55dB of rejection required in the image band up to 18GHz. Above this frequency a repeat response of the passband occurs which causes a decrease in stopband attenuation.

6.8 Summary

In this chapter two filter designs were investigated as suitable filters to be used by both the direct digitization as well as the heterodyne receivers. The first design was based on a quasi-lumped element design, while the second being a distributed design using transmission lines. The quasi-lumped element design required the implementation of capacitor and inductors values which is smaller than that which can be implemented on SSL. This design was therefore abandoned.

A distributed filter was designed and constructed using micro-strip substrate. Apart from additional losses in the passband, this filter met all the rejection requirements of both the anti-aliasing as well as the image reject filter up to 18GHz where after the repeat response of this filter caused a reduction in the stopband rejection. This resulted in this filter not meeting the rejection specification over the entire image band.

In an attempt to minimize the losses in the passband, the same filter design was implemented in SSL. This design resulted in a significant improvement in passband losses. Unfortunately an unexplained decrease in stopband attenuation resulted in this filter not meeting the required stopband rejection over the image band. A comparison of the ideal filter to that of the micro-strip and SSL filters was presented in figure 6.21. In the next chapter the effect of the filter response on the system is discussed.

Chapter 7

System Verification

In this chapter the effect of the filter performance on the direct digitizing as well as the heterodyne receiver is investigated. During this investigation an ideal filter is firstly integrated with the receiver to determine the ideal receiver performance. The performance of the ideal receiver is then compared to a receiver fitted with micro-strip filter with a frequency response as shown in figure 6.21.

7.1 Direct Digitization Receiver

The test configuration used to evaluate the filter performance on the direct digitizing receiver is shown in figure 7.1 as modelled in AWR software[25]. A test signal as well as noise is applied to a filter before being digitized and scaled by the ADC. Two measurement test points are configured in this test setup. TP1 measures the power spectrum at the output of the anti-aliasing filter. TP2 measures the power spectrum at the output of the ADC. The anti-aliasing filter can be selected to be either an ideal distributed filter or the micro-strip filter designed in this thesis.

The output spectra produced by the two receiver configurations are captured

and compared for a test signal frequency of 6, 14.5 and 21.5 GHz. The 6 GHz test signal is at baseband. The 14.5 GHz signal is at the upper frequency of the passband. The 21.5 GHz test signal is chosen to be within the 2nd Nyquist zone at the peak of the repeat response generated by the micro-wave filter. The results of the 6 GHz test signal for the ideal receiver is shown in figure 7.2 and the corresponding results for the receiver with the designed filter shown in figure 7.3. In both these cases the out of band 6 GHz signal is sufficiently attenuated by both filters such that no signal is produced in the output spectrum. The spectrum produced by the in band 14.5 GHz test signal is shown for both test cases in figures 7.4 and 7.5 respectively. The 14.5 GHz folds to baseband and is produced at 0.5 GHz in the output spectrum of the ADC. The only difference in the spectra is a difference in the peak power of the 0.5GHz signal. This difference in power is due to the insertionloss added by the micro-strip filter. The results of the final test case of 21.5 GHz is shown in figures 7.6 and 7.7. For the ideal filter test case, the out of band 21.5 GHz signal is not visible in either the spectrum produced at the output of the anti-alias filter or the output of the ADC. The ideal filter completely rejects this out of band signal. In the case of the micro-strip filter, the filter does not reject the out of band signal resulting in this signal aliasing to baseband and is produced at 6.5 GHz. This signal will be indistinguishable from an in band signal located at 8.5 GHz.

It is clear from these tests that the repeat responses generated by the designed micro-strip filter will cause unwanted aliasing of out of band signals in the 2nd Nyquist zone. According to the measured frequency response of this filter presented in figure 6.21, the frequency at which this will exceed the system specifications is approximately 20 GHz. Other components in the signal chain can however be used to suppress signals above 20GHz. The ADC [23] for example only has an RF bandwidth of 20GHz. Similarly a typical LNA that can be used for this application only has a RF bandwidth of 4 to 16 GHz [38]. It is therefore unlikely that this repeat response will be a problem in the final design. Signals at baseband are sufficiently rejected by the designed filter. Signals within the passband are attenuated by the insertionloss of the designed filter as expected. The designed filter therefore can meet the rejection requirements of anti-aliasing

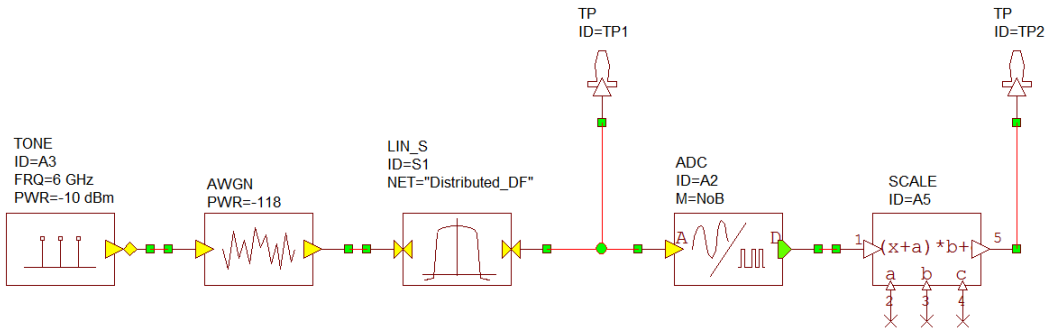

Figure 7.1: Test configuration for direct digitizing receiver.

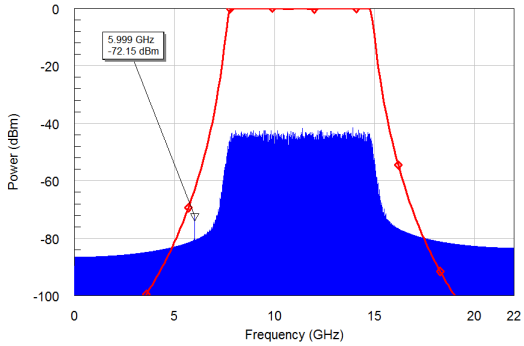

(a) Anti-alias filter output (blue). Anti-alias filter frequency response (red).

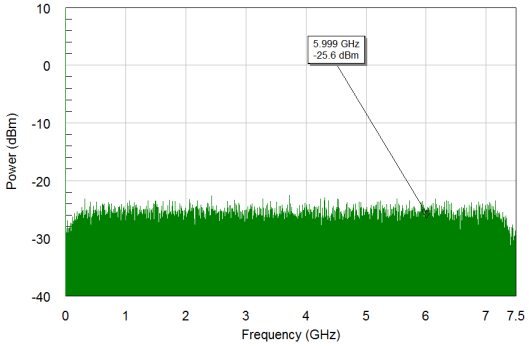

(b) Digitizer output.

Figure 7.2: Rejection of 6 GHz interfering signal by ideal Direct digitization receiver.

filter required by the direct digitizing receiver.

7.2 Heterodyne Receiver

The test configuration used to evaluate the filter performance on the heterodyne receiver is shown in figure 7.8 also modelled in AWR software[25]. Similar to the test done for the direct digitizing receiver a test signal as well as noise is injected to the input of the receiver. In this test configuration the first test point, labelled "Input", is configured to measure the output power spectrum of the image reject filter. The second test point, labelled "Output", is configured to measure the

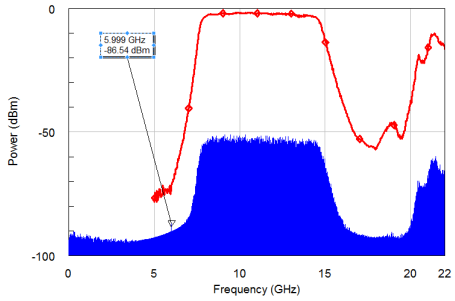

(a) Anti-alias filter output (blue). Anti-alias filter frequency response (red).

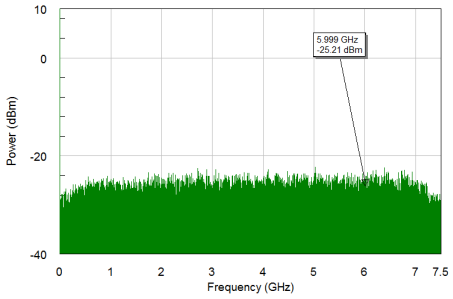

(b) Digitizer output.

Figure 7.3: Rejection of 6 GHz interfering signal by ideal Direct digitization receiver.

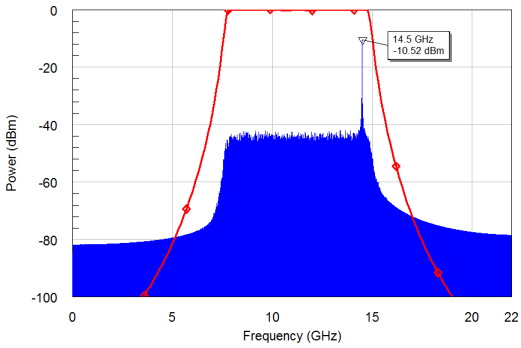

(a) Anti-alias filter output (blue). Anti-alias filter frequency response (red).

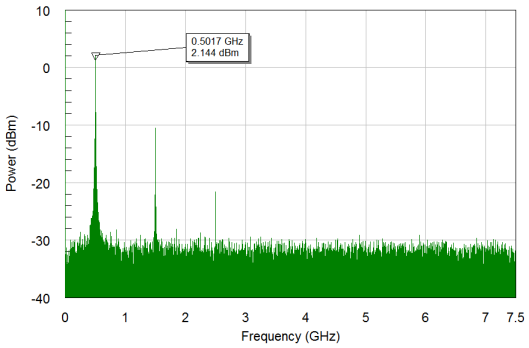

(b) Digitizer output.

Figure 7.4: Rejection of 14.5 GHz interfering signal by ideal Direct digitization receiver.

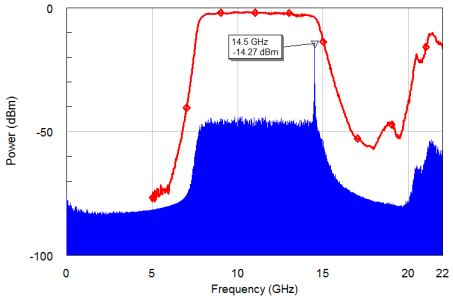

(a) Anti-alias filter output (blue). Anti-alias filter frequency response (red).

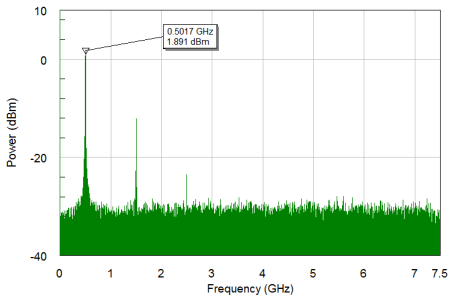

(b) Digitizer output.

Figure 7.5: Rejection of 14.5 GHz interfering signal by Direct digitization receiver.

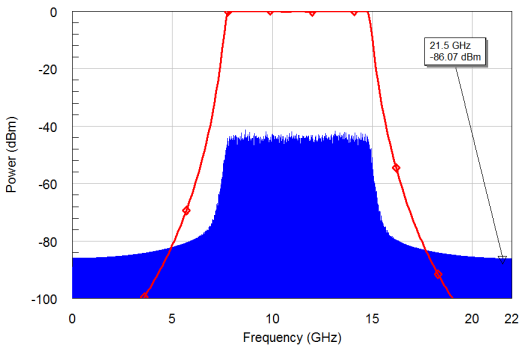

(a) Anti-alias filter output (blue). Anti-alias filter frequency response (red).

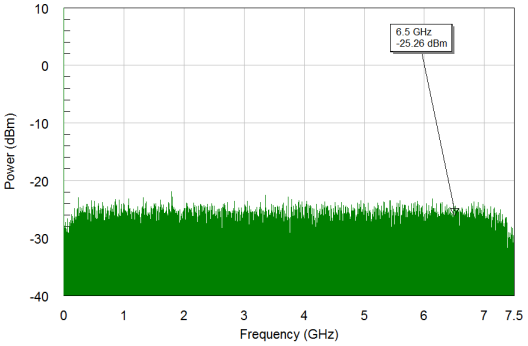

(b) Digitizer output.

Figure 7.6: Rejection of 21.5 GHz interfering signal by ideal Direct digitization receiver.

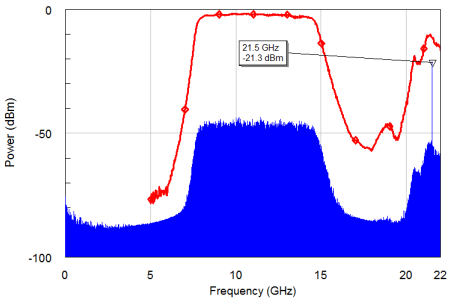

(a) Anti-alias filter output (blue). Anti-alias filter frequency response (red).

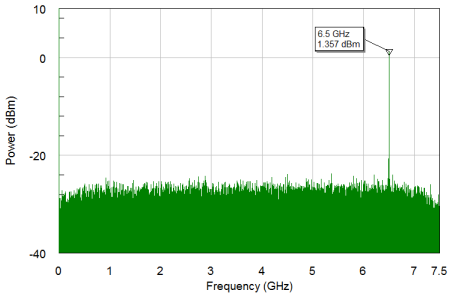

(b) Digitizer output.

Figure 7.7: Rejection of 21.5 GHz interfering signal by Direct digitization receiver.

power spectrum at the IF of the receiver. The image reject filter can be selected to be either an ideal distributed filter or the designed micro-strip filter.

Again the output spectra produced by the two receiver configurations are captured and compared for a test signal frequency of 6, 14.5 and 21.5 GHz. The LO frequency is adjusted to select the lower 2.5 GHz of the passband (8 -10.5 GHz) for the 6 GHz test case. For both the 14.5 and 21.5 GHz test cases the LO is tuned to select the upper 2.5 GHz (12-14.5 GHz) section of the band. The 21.5 GHz test signal is selected to be within the image range of the receiver. It is also selected to be on the repeat response of the designed filter.

The results of the 6 GHz test signal for the ideal receiver is shown in figure 7.9 and the corresponding results for the receiver with the designed filter shown in figure 7.10. This out of band signal is is not expected to be present in the IF spectrum as the downconverted signal will be outside the IF bandwidth. This is confirmed by the IF spectra produced for both receiver configurations. The spectrum produced by the in band 14.5 GHz test signal is shown for both test cases in figures 7.11 and 7.12 respectively. The 14.5 GHz is downconverted to 3.25 GHz as expected. The only difference in the IF spectra produced is a difference in the peak power produced by these receivers. This difference is as a result of the difference in insertionloss between the ideal filter and the designed filter.

The results of the final test case of 21.5 GHz is shown in figures 7.13 and 7.14. For the ideal filter test case, the out of band 21.5 GHz signal is not visible in either the spectrum produced at the output of the image reject filter or the IF. The ideal filter completely rejects this out of band signal. In the case of the micro-strip filter, the filter does not reject the out of band signal resulting in this signal mixing down to the IF frequency of 3.75GHz. This is due to the 21.5 GHz signal being located in the image frequency range of the receiver. This signal will be indistinguishable from an in band signal located at 14 GHz. According to the measured frequency response of this filter presented in figure 6.21, the frequency at which the designed filter does not meet the image reject requirements is approximately 18 GHz. As in the case of the direct digitzing receiver, other components in the signal chain can suppress signals above 18GHz. A suitable mixer which has been identified

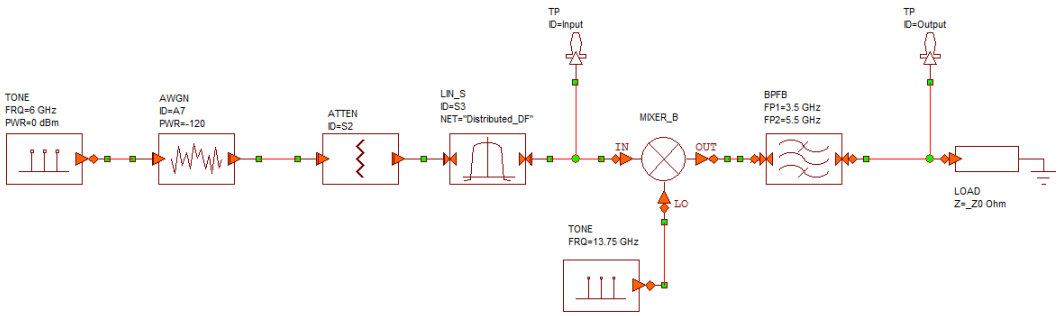

Figure 7.8: Test configuration for heterodyne receiver.

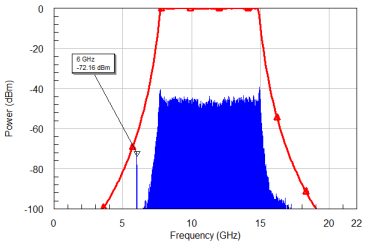

(a) Image reject filter output spectrum (blue). Image reject filter frequency response (red).

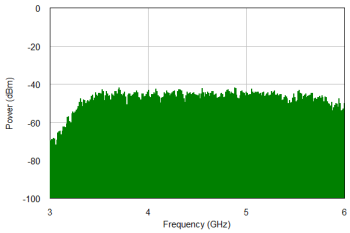

(b) IF output spectrum.

Figure 7.9: Rejection of 6 GHz interfering signal by heterodyne receiver with ideal image reject filter.

for this application is a balanced mixer from MACOM [39]. The frequency range of the RF port of this mixer is 2 to 18 GHz. In addition to this the same LNA proposed for the direct digitization receiver can be used. The RF bandwidth of this LNA is 4 to 16 GHz [38]. These components will provide additional rejection of the image range. The exact amount of rejection will depend on the final design implementation.

7.3 Summary

In this chapter the effect of the designed filter on the performance of the direct digitization as well as the heterodyne receiver is verified. This verification was

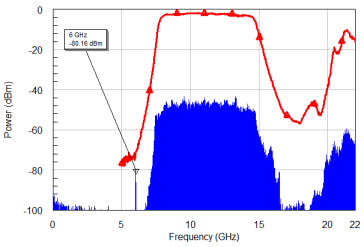

(a) Image reject filter output spectrum (blue). Image reject filter frequency response (red).

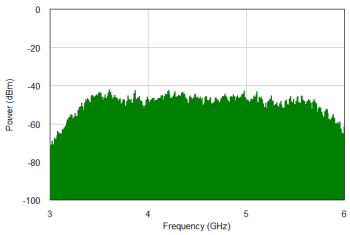

(b) IF output spectrum.

Figure 7.10: Rejection of 6 GHz interfering signal by heterodyne receiver with designed filter.

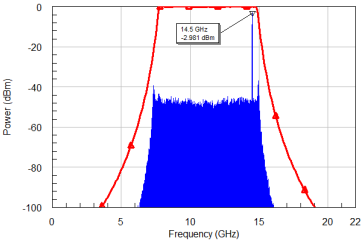

(a) Image reject filter output spectrum (blue). Image reject filter frequency response (red).

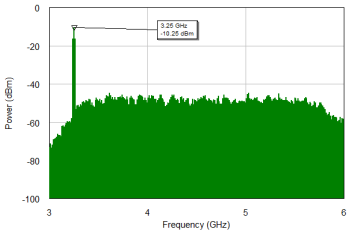

(b) IF output spectrum.

Figure 7.11: Downconversion of 14.5 GHz signal by heterodyne receiver with ideal image reject filter.

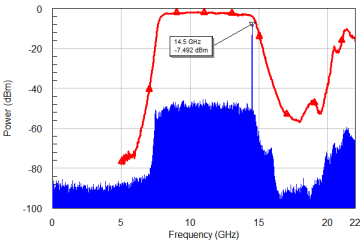

(a) Image reject filter output spectrum (blue). Image reject filter frequency response (red).

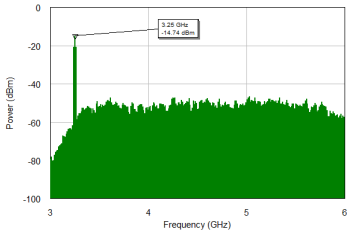

(b) IF output spectrum.

Figure 7.12: Downconversion of 14.5 GHz signal by heterodyne receiver with designed filter.

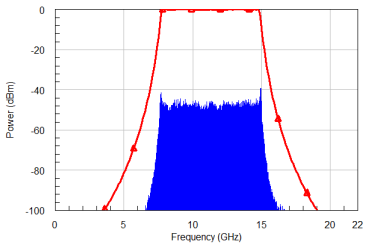

(a) Image reject filter output spectrum (blue). Image reject filter frequency response (red).

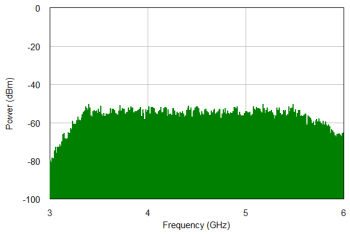

(b) IF output spectrum.

Figure 7.13: Rejection of 21.5 GHz interfering signal by heterodyne receiver with ideal filter.

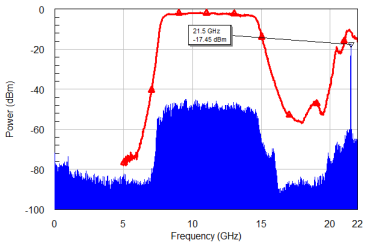

(a) Image reject filter output spectrum (blue). Image reject filter frequency response (red).

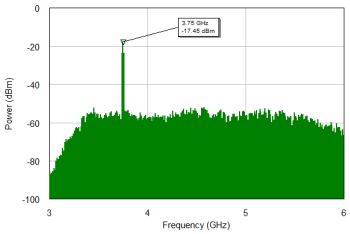

(b) IF output spectrum.

Figure 7.14: Rejection of 21.5 GHz interfering signal by heterodyne receiver with designed filter.

done by comparing the output spectrum produced by both these types of receivers when using an ideal filter compared to the spectrum produced using the designed filter. The results show that the designed filter meets the specifications for both the anti-aliasing and image reject filters. The repeat response of the designed filter does however result in signals located in the 2nd Nyquist zone of the direct digitizing receiver not being sufficiently rejected. Similarly signals located in the image range of the heterodyne receiver are also not sufficiently rejected. Additional rejection over these frequency ranges will however be provided by other components such as the LNA, mixer and ADC resulting compliance at a system level.

Chapter 8

Conclusions and Future Work

8.1 Conclusions

Two receiver architecture options for digitizing the extended X-band spectrum for MeerKAT has been proposed in this thesis. The first option was a direct digitization receiver. The second option was to downconvert 2.5GHz portions of the MeerKAT band to a suitable IF using a single stage heterodyne receiver. Both of these options were found to be viable, although the direct digitization receiver require an ADC that can sample at 15 Gsps. An ADC has been identified which can sample at this rate, but this ADC only produces 3 bits at every sample which might not be enough to meet the dynamic range requirement of the radio telescope. The heterodyne receiver can be constructed using readily available current technology. This architecture is however more complex and expensive compared to that of the direct digitization receiver.

Both these receivers require a band select filter at the input of the receiver. In the case of the direct digitization receiver, the band select filter is actually an anti-aliasing filter. In the case of the heterodyne receiver, the band select filter is an image reject filter.

Two microwave filter designs was investigated for possible implementation of

both the anti-alias filter as well as the image reject filter required for these options. The first design that was investigated was a quasi-lumped element design implemented on SSL. The second design was an optimum distributed bandpass filter. The capacitance and inductance required for the quasi-lumped element design could however not be implemented on SSL due to parasitic capacitance. This filter design was therefore found to be not suitable for this application. The optimum distributed bandpass filter design used transmission lines which could easily be implemented on micro-strip. This filter was designed and manufactured. The filter met all specifications except for a repeat response in the upper stopband of the filter. The frequency of this repeat response falls within the 2nd Nyquist zone of the direct digitization receiver. It also falls within the image rejection range of the heterodyne receiver. The effect of this repeat response on the performance of both receiver architectures was verified. It was found that that this response will cause unwanted aliasing in the direct digitization receiver. It will also cause an unwanted image to appear at the IF of the heterodyne receiver. Fortunately the bandwidth limitation of other components in signal chain such as the LNA, mixer and ADC will sufficiently suppress this response resulting in compliance at a system level.

8.2 Future Work

Although the objectives of this thesis have been met, two interesting future work activities have been identified. These are listed below:

- In section 6.6 the distributed filter was designed and constructed using micro-strip technology. This resulted in the width of transmission lines being fairly thin. In an attempt to increase these line widths, this design was implemented on SSL. The simulated frequency response of the SSL design was very close to that of an ideal filter except for an unexplained response in the stopband. The cause of this response must be investigated as a future work activity.

- The quasi-lumped element filter design in section 6.1.1 was found not to be suitable for the anti-aliasing and image reject filter design. A quasi-lumped element filter can however be ideally suited for the anti-aliasing filter required by the heterodyne receiver which is centered at 4.5 GHz and has bandwidth of 2.5 GHz. The design of such a filter can be done as a future work activity.

Appendix A: Suspended Strip-line Impedance calculation

The typical layout of a Suspended Strip Line (SSL) structure is shown in the figure ref 1 below:

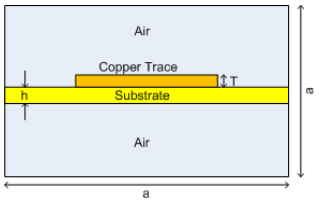

Figure 1: Suspended Strip Line (SSL) structure.

The impedance of such a SSL transmission line is can be calculated using the following design equations [40]. For designs where $a/2 < W < a$:

$$Z_0 = \eta_0 \left[V + \frac{R}{\frac{W}{b} + 0.6670\, ln\left(\frac{W}{b} + 1.444\right)} \right] \tag{1}$$

$$\varepsilon_{eff} = \frac{1}{[1 + (E - (Fln\frac{w}{b})ln(\frac{1}{\sqrt{\varepsilon_r}}))]^2} \tag{2}$$

$$V = -0.6301 - 0:07082\frac{h}{b} + 0.247\frac{a}{b} \quad (3)$$

$$R = 1.9492 + 0.1553\frac{h}{b} - 0.5123\frac{a}{b} \quad (4)$$

$$E = 0.464 + 0.9647\frac{h}{b} - 0.2063\frac{a}{b} \quad (5)$$

$$F = -0.1424 + 0.3017\frac{h}{b} + 0.02411\frac{a}{b} \quad (6)$$

For designs where $0 < W < a/2$:

$$Z_0 = \frac{\eta_0}{2\pi}\left[V + Rln\left(\frac{6}{W/b} + \sqrt{1 + \frac{4}{(W/b)^2}}\right)\right] \quad (7)$$

and

$$\varepsilon_{eff} = \frac{1}{[1 + (E - (Fln\frac{w}{b})ln(\frac{1}{\sqrt{\varepsilon_r}}))]^2} \quad (8)$$

where

$$V = 1.7866 - 0.2035\frac{h}{b} + 0.4750\frac{a}{b} \quad (9)$$

$$R = 1.0835 + 0.1007\frac{h}{b} - 0.09457\frac{a}{b} \quad (10)$$

$$E = 0.2077 + 1.2177\frac{h}{b} - 0.08364\frac{a}{b} \quad (11)$$

$$F = 0.03451 - 0.1031\frac{h}{b} + 0.01742\frac{a}{b} \quad (12)$$

The resultant impedance curve for the structure described in chapter 6 is shown in figure 2. The effective dielectric constant as a function of trace width is shown in figure 3. These curves are generated for a design using Mercurywave 9350 211 μm thick substrate.The copper thickness is 35 μm and the evaluation frequency is 15.6GHz.

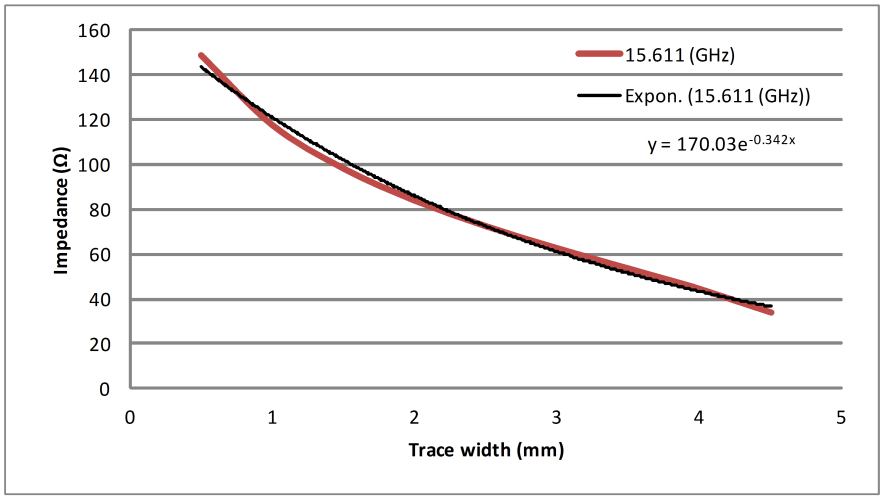

Figure 2: Simulated impedance as a function of trace width for SSL at 15.611GHz. *Equation provides approximation of width vs. impedance.*

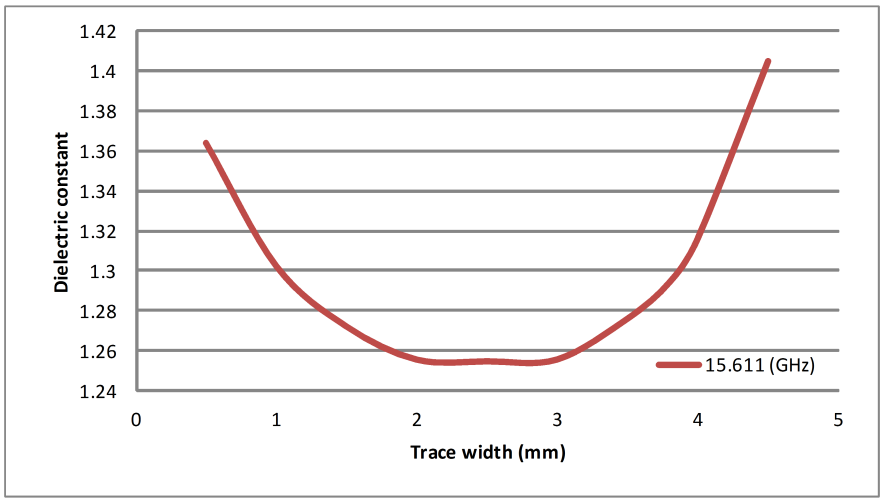

Figure 3: Simulated ε_{eff} as a function of trace width for SSL structure at 15.611 GHz.

Appendix B: UCT Ethics Clearance

Application for Approval of Ethics in Research (EiR) Projects
Faculty of Engineering and the Built Environment, University of Cape Town

APPLICATION FORM

Please Note:
Any person planning to undertake research in the Faculty of Engineering and the Built Environment (EBE) at the University of Cape Town is required to complete this form **before** collecting or analysing data.The objective of submitting this application *prior* to embarking on research is to ensure that the highest ethical standards in research, conducted under the auspices of the EBE Faculty, are met. Please ensure that you have read, and understood the **EBE Ethics in Research Handbook**(available from the UCT EBE, Research Ethics website) prior to completing this application form: http://www.ebe.uct.ac.za/usr/ebe/research/ethics.pdf

APPLICANT'S DETAILS		
Name of principal researcher, student or external applicant		Jocias A Malan
Department		Electrical Engineering
Preferred email address of applicant:		sias@ska.ac.za
If a Student	Your Degree: e.g., MSc, PhD, etc.,	MSc
	Name of Supervisor (if supervised):	Prof Riana Geschke
If this is a researchcontract, indicate the source of funding/sponsorship		SKA South Africa/ NRF
Project Title		Systems design of a X-band receiver for MeerKAT Telescope

I hereby undertake to carry out my research in such a way that:

- there is no apparent legal objection to the nature or the method of research; and
- the research will not compromise staff or students or the other responsibilities of the University;
- the stated objective will be achieved, and the findings will have a high degree of validity;
- limitations and alternative interpretations will be considered;
- the findings could be subject to peer review and publicly available; and
- I will comply with the conventions of copyright and avoid any practice that would constitute plagiarism.

SIGNED BY	Full name	Signature	Date
Principal Researcher/ Student/External applicant	Jocias Alexander Malan	Signed	12/01/2017 Click here to enter a date.

APPLICATION APPROVED BY	Full name		Date
Supervisor (where applicable)	Prof Riana Geschke		12/01/17 Click here to enter a date.
HOD (or delegated nominee) Final authority for all applicants who have answered NO to all questions in Section1; and for all Undergraduateresearch (Including Honours).	E Boyce Click here to enter text.		3/3/17 Click here to enter a date.
Chair : Faculty EIR Committee For applicants other than undergraduate students who have answered YES to any of the above questions.	Click here to enter text.		Click here to enter a date.

References

[1] P. Pratap and G. McIntosh, "Measurement of the radiation from thermal and nonthermal radio sources," *American Journal of Physics*, vol. 73, no. 5, pp. 399–404, 2005. vii, 12, 13

[2] Wikipedia, "Copyrighted free use, https://commons.wikimedia.org." Wikipedia, 2017. vii, 15

[3] "Square kilometre array, south africa." http://www.ska.ac.za/. Accessed: 2016-08-20. 1, 8

[4] J. M. A.R. Thompson and G. S. Jr., *Interferometry and Synthesis in Radio Astronomy*. Wenheim, Germany: Wiley-VCH, 2004. 4, 6, 7, 9, 10, 12, 13

[5] "Physics of the universe: Cosmic background radiation.." http://www.physicsoftheuniverse.com/. Accessed: 2016-11-30. 5

[6] "High energy stereoscopic system." https://www.mpi-hd.mpg.de/hfm/HESS/. Accessed: 2016-11-01. 5

[7] "Arecibo observatory, puerto rico." http://www.naic.edu/. Accessed: 2016-11-01. 6

[8] "Karl g. jansky very large array." http://www.vla.nrao.edu/. Accessed: 2016-11-01. 7

[9] "Square kilometre array." http://www.skatelescope.org. Accessed: 2016-08-20. 8

[10] C. Granet, "Designing classical offset cassegrain or gregorian dual-reflector antennas from combinations of prescribed geometric parameters," *IEEE Antennas and Propagation Magazine*, vol. 44, pp. 114–123, Jun 2002. 8

[11] J. D. Kraus, *Antennas*. New York, USA: Tata McGraw-Hill, 1988. 8, 20

[12] S. G. et. al, "Meergal: A meerkat high frequency galactic plane survey." SKA SA Internal document, 2015. 12

[13] M. Giavalisco, "Galaxies at high redshift." Encyclopedia of Astronomy and Astrophysics, 2006. 14

[14] A. Peens-Hough, "Receptor description and requirements." SKA SA Internal document, 2016. 21, 25, 26, 28, 30, 41

[15] R. J. Halligan, "Requirements analysis and specification writing." Course notes, 2010. 23

[16] D. A. T. et al, "Republic of south africa: Proposal to host the square kilometere array." SKA SA Internal document, 2006. 24

[17] "Radio frequencies for space communication.." http://www.spaceacademy.net.au/spacelink/radiospace.htm. Accessed: 2016-12-15. 25

[18] J.-S. Hong and M. Lancaster, *Microstrip Filters for RF/Microwave Applications*. New York, USA: John Wiley and Sons, Inc, 2012. 25, 60, 62, 63, 65

[19] D. M. Pozar, *Microwave Engineering*. New York, USA: John Wiley and Sons, Inc, 2004. 27, 29, 30, 47, 48, 50, 52, 59, 65

[20] R. Boute, "The geometry of bandpass sampling: A simple and safe approach [lecture notes]," *IEEE Signal Processing Magazine*, vol. 29, pp. 90–96, July 2012. 32, 33, 35, 37

[21] C.-H. Tseng and S.-C. Chou, "Direct downconversion of multiple rf signals using bandpass sampling," in *Communications, 2003. ICC '03. IEEE International Conference on*, vol. 3, pp. 2003–2007 vol.3, May 2003. 35

[22] R. G. Vaughan, N. L. Scott, and D. R. White, "The theory of bandpass sampling," *IEEE Transactions on Signal Processing*, vol. 39, pp. 1973–1984, Sep 1991. 35

[23] A. Devices, "Hmcad5831lp9be." Datasheet, 2017. 38, 79

[24] S. M. et. al, "Meerkat digitiser design document." SKA SA Internal document, 2016. 40

[25] N. Instruments, "National instruments awr design environment." Software, 2016. 41, 55, 61, 63, 65, 68, 78, 80

[26] B. C. Henderson, "Mixers in microwave systems." Tech-note: WJ Communications, Inc., 2010. 48

[27] "e2v adc product guide." http://www.e2v.com/products/semiconductors/adc/. Accessed: 2016-11-30. 52

[28] "Adsantec adc product guide." http://www.adsantec.com/41-analog-digital-signal-converters. Accessed: 2016-11-30. 52

[29] ITU, "International telecommunication union (itu) radiocommunications sector." Standard, 2017. 58

[30] W. Menzel, "A novel miniature suspended stripline filter," in *2003 33rd European Microwave Conference*, pp. 1047–1050, Oct 2003. 59

[31] W. Menzel, M. S. R. Tito, and L. Zhu, "Low-loss ultra-wideband (uwb) filters using suspended stripline," in *2005 Asia-Pacific Microwave Conference Proceedings*, vol. 4, pp. 4 pp.–, Dec 2005. 59, 71

[32] W. Menzel and A. Balalem, "Quasi-lumped suspended stripline filters and diplexers," *IEEE Transactions on Microwave Theory and Techniques*, vol. 53, pp. 3230–3237, Oct 2005. 59, 60

[33] Z. Zakaria, M. A. Mutalib, and A. B. Jiim, "A compact and systematic design of microstrip and suspended stripline structure (sss) bandpass filter with defected structure for wideband applications," in *Recent Advances in Mathematical and Computational Methods*, pp. 66–75, Oct 2015. 62

[34] J. Malherbe, *Microwave Transmission Line Filters*. Massachusetts, USA: Artech House, Inc., 1979. 62

[35] P. electrochemical corporation, "Mercury wave 9350 substrate datasheet." Datasheet, 2017. 65, 73

[36] SONNET, "Sonnet software 16.52." Software, 2016. 68

[37] CST, "Computer simulation technology (cst)." Software, 2016. 74

[38] L. N. Factory, "4-16ghz cryogenic low noise amplifier." Datasheet, 2014. 79, 84

[39] MACOM, "My85c datasheet." Datasheet, 2017. 84

[40] A. Lehtovuori and L. Costa, "Model for shielded suspended substrate microstrip line," in *Circuit Theory Laboratory Report Series*, pp. 1–2, Oct 1998. 91